Clim Dyn (2014) 43:1753–1772
DOI 10.1007/s00382-013-2003-6

Sensitivity of the regional climate model RegCM4.2 to planetary boundary layer parameterisation

Ivan Güttler · Čedo Branković · Travis A. O'Brien · Erika Coppola · Branko Grisogono · Filippo Giorgi

Received: 26 April 2013 / Accepted: 13 November 2013 / Published online: 27 November 2013

Abstract This study investigates the performance of two planetary boundary layer (PBL) parameterisations in the regional climate model RegCM4.2 with specific focus on the recently implemented prognostic turbulent kinetic energy parameterisation scheme: the University of Washington (UW) scheme. When compared with the default Holtslag scheme, the UW scheme, in the 10-year experiments over the European domain, shows a substantial cooling. It reduces winter warm bias over the north-eastern Europe by 2 °C and reduces summer warm bias over central Europe by 3 °C. A part of the detected cooling is ascribed to a general reduction in lower tropospheric eddy heat diffusivity with the UW scheme. While differences in temperature tendency due to PBL schemes are mostly localized to the lower troposphere, the schemes show a much higher diversity in how vertical turbulent mixing of the water vapour mixing ratio is governed. Differences in the water vapour mixing ratio tendency due to the PBL scheme are present almost throughout the troposphere. However, they alone cannot explain the overall water vapour mixing ratio profiles, suggesting strong interaction between the PBL and other model parameterisations. An additional 18-member ensemble with the UW scheme is made, where two formulations of the master turbulent length scale in unstable conditions are tested and unconstrained parameters associated with (a) the evaporative enhancement of the cloud-top entrainment and (b) the formulation of the master turbulent length scale in stable conditions are systematically perturbed. These experiments suggest that the master turbulent length scale in the UW scheme could be further refined in the current implementation in the RegCM model. It was also found that the UW scheme is less sensitive to the variations of the other two selected unconstrained parameters, supporting the choice of these parameters in the default formulation of the UW scheme.

Keywords Eddy heat diffusivity · Structural uncertainty · RegCM · Systematic errors

Electronic supplementary material The online version of this article (doi:10.1007/s00382-013-2003-6) contains supplementary material, which is available to authorized users.

I. Güttler (✉) · Č. Branković
Croatian Meteorological and Hydrological Service (DHMZ), Grič 3, 10 000 Zagreb, Croatia
e-mail: ivan.guettler@cirus.dhz.hr

T. A. O'Brien
Earth Sciences Division, Lawrence Berkeley National Lab, Berkeley, CA, USA

E. Coppola · F. Giorgi
Earth System Physics Section, International Centre for Theoretical Physics (ICTP), Strada Costiera 11, Trieste, Italy

B. Grisogono
Department of Geophysics, Faculty of Science, University of Zagreb, Horvatovac 95, Zagreb, Croatia

1 Introduction

Turbulent eddies in the planetary boundary layer (PBL) strongly influence vertical fluxes of momentum, heat and mass between the surface and the atmosphere. Although the spatial and temporal scales of turbulent eddies are several orders of magnitude smaller than the climatologically relevant scales, sensible and latent heat fluxes due to turbulent eddies are major components of the global energy budget (Trenberth et al. 2009). The PBL also acts as a sort of interactive buffer zone between the underlying surface and the free atmosphere, and therefore an understanding of the coupling between the PBL and the land

surface is of particular concern. Climatological aspects of observed and model simulated PBL do not receive much attention in scientific literature, even though two of the most often analysed variables in climate studies, near-surface temperature (*T2m*) and precipitation, are controlled by the PBL processes (e.g. Giorgi et al. 1993; Dethloff et al. 2001; Shin and Ha 2007; Esau and Zilitinkevich 2010).

Substantial differences in spatial resolution of numerical models and spatial scale of atmospheric turbulent eddies ($\sim$10–100 km vs. $\sim$10–1,000 m) require that the impact of turbulent eddies on resolved model flow must be parameterised (e.g. Stewart 1979). Because of strong interaction between PBL processes and surface processes, the fidelity of various feedbacks in models [such as the snow-albedo feedback (Winton 2006) and the methane feedback (Walter et al. 2006)] can be tied to the fidelity of the PBL parameterisation. An analysis of the PBL effects on climatological scales simulated by global or regional climate models (GCMs and RCMs respectively) typically includes bulk measures of turbulent activity, such as the PBL height and turbulent kinetic energy (TKE) and the validation of surface fluxes due to turbulent eddies (e.g. Medeiros et al. 2005; Sánchez et al. 2007; Jaeger et al. 2009). From available literature, it appears that none of the currently available PBL parameterisation schemes are generally superior and that the use and design of a specific scheme is often in the function of application (Wyngaard 1985; Grenier and Bretherton 2001; Zhu et al. 2005; Cuxart et al. 2006). Additionally, there is often a substantial time lag between the accepted knowledge of the PBL physics and its implementation in atmospheric and climate models (Baklanov et al. 2011).

Most PBL schemes can be broadly grouped into *non-local* and *local* types of schemes (e.g. Stensrud 2007). The term *non-local* refers to the schemes that use global characteristics of PBL (e.g. the PBL height) to express the turbulent fluxes, and the term *local* refers to the schemes that use local characteristics of PBL (e.g. vertical gradients of the mean PBL properties). Intercomparison of various PBL schemes in limited area models is a subject of many studies, most of them conducted for MM5[1] and WRF[2] models in simulations ranging from several hours to several months. Substantial spread in these simulations is found when changing the PBL scheme, often linked with differences in the vertical mixing strength and the entrainment of the above-PBL air (e.g. Hu et al. 2010; Xie et al. 2012; García-Díez et al. 2013).

[1] PSU/NCAR Mesoscale Model, version 5, Pennsylvania State University and National Center for Atmospheric Research, USA.

[2] Weather Research and Forecasting community model (http://www.wrf-model.org).

In this study, we examine the impact of the two PBL schemes on simulated climatology over Europe in the regional climate model RegCM4.2 (Giorgi et al. 2012): the non-local diagnostic PBL scheme (the Holtslag scheme; Holtslag et al. 1990; Holtslag and Boville 1993), and the recently implemented local prognostic 1.5-order scheme (the University of Washington or the UW scheme; Grenier and Bretherton 2001). The Holtslag scheme has been a part of the RegCM model since the RegCM2 and its impact on the model 1-month "climatology" was explored by Giorgi et al. (1993). The implementation of the UW scheme in RegCM4 is documented in O'Brien et al. (2012) and the initial comparisons between the two PBL schemes are described in O'Brien et al. (2012) and Giorgi et al. (2012).

The aim of this study is to investigate the structural uncertainty of RegCM4.2 related to PBL schemes. Here, the term "structural uncertainty" refers to uncertainty in the design of climate models that results from the fact that physical process can be represented in numerical models in various ways (e.g. Stainforth et al. 2007; Tebaldi and Knutti 2007; Curry and Webster 2011). First, model sensitivity to the two different PBL schemes is analyzed and possible mechanisms that explain the differences in vertical profiles of temperature and water vapour mixing ratio are proposed. Second, sensitivity of the UW scheme alone will be analyzed in a perturbed physics ensemble (PPE). Here, we perturb two unconstrained parameters in the UW scheme and evaluate the impact of two simple formulations of the master turbulent length scale. These perturbations are introduced one at a time, thus clearly identifying the impact of each combination of perturbed parameters. The presence of unconstrained and tuneable parameters is the consequence of our incomplete knowledge of physical processes involved or simplifications in any atmospheric model. The range of variation for most parameters in both PBL schemes is determined from observations and/or idealized high-resolution simulations (e.g. large-eddy simulations in Grenier and Bretherton 2001). GCM studies that use PPEs to systematically analyze model sensitivity are fairly common (e.g. Murphy et al. 2004; Stainforth et al. 2005; Zhang et al. 2012), while the PPE studies for RCMs are still rarely performed (e.g. Suklitsch et al. 2011; Bellprat et al. 2012).

Although RegCM is a commonly used model, there has not yet been a study of its structural uncertainty by either performing a large ensemble of many various combinations of parameterisations or by varying unconstrained parameters in a large PPE for an extended simulated period. However, there is a growing set of studies analyzing the RegCM structural uncertainty either through changing a subset of parameterisations or through customizing and perturbing the values of a few unconstrained parameters. They include studies on the impact of, for example, cloud

microphysics (Pal et al. 2000), convective parameterisations (e.g. Yang and Arritt 2002; Davis et al. 2009; Gianotti et al. 2012), land-surface processes (Steiner et al. 2005, 2009; Winter et al. 2009; Gianotti et al. 2012) and PBL processes (e.g. Giorgi et al. 1993; O'Brien et al. 2012). An overview of representative studies relevant for the RegCM PBL structural uncertainties indicates the lack of a common analysis strategy (e.g. choice of domain, model version or selected variables) thus making it difficult for their results to be generalized. Furthermore, the use of more advanced parameterisation does not automatically improve model performance in all variables. Our study contributes towards a better understanding of structural uncertainties in the RegCM model that may arise from the rarely explored PBL parameterisation. It is ordered as follows: in Sect. 2 we describe the experimental setup and the two PBL schemes and justify the choices in PPE of the UW simulations; in Sect. 3, the near-surface climatology in the two 10-year simulations are compared and discussed (the Holtslag vs. the UW scheme); in Sect. 4, an intercomparison of vertical profiles for various climate fields is given, followed by an analysis of the PPE in the UW simulations (the 18-member ensemble of UW simulations) in Sect. 5; in Sect. 6, a summary and suggestions for possible directions of future work are presented. In Supplement 1, supporting material for the intercomparison of vertical profiles is provided; in Supplement 2, an evaluation of the RegCM sensible and latent heat fluxes against ERA-Interim and the observations from the C-SRNWP Project is presented and discussed.

2 Method

We use monthly mean temperature at 2 m (*T2m*) and precipitation from the CRU[3] TS 3.0 dataset (Mitchell and Jones 2005) available at 0.5° × 0.5° grid to validate the model's *T2m* and precipitation. This observational dataset is used to examine model errors of the mean seasonal fields in simulations with both PBL schemes. Methodology and datasets for evaluation of sensible and latent heat fluxes are presented in Supplement 2.

The version of the model used is RegCM4.2[4] (Giorgi et al. 2012). The model setup includes a 50-km horizontal resolution and 23 vertical levels with the model top at 50 hPa. The boundary conditions are provided by the ERA-Interim reanalysis (Dee et al. 2011) from 1989 to 1998 in the two experiments, and from 1989 to 1991 in the 18 PPE experiments (Table 1). The integration domain includes Europe and the northern Africa (Fig. 1). The following parameterisations of the subgrid processes are used in all experiments: the BATS1e scheme for the land-surface processes (Dickinson et al. 1993), the Pal et al. (2000) parameterisation of large-scale precipitation and clouds, the Emanuel (1991) scheme for deep convection and the scheme for longwave and shortwave radiation transfer from Kiehl et al. (1996). The model has two PBL schemes implemented: the Holtslag scheme (Holtslag et al. 1990;

Table 1 Experiments, the values of perturbed parameters a_2 (Eq. 11) and R_{STBL} (Eq. 8) and the choice of the formulation for the master turbulent length scale (Eqs. 6, 7)

Exp	PBL scheme	Master turbulent length scale	Efficiency of evaporative enhancement of cloud-top entrainment a_2	Scaling parameter in stable boundary layer turbulent length scale R_{STBL}
001	Holtslag	–	–	–
002	UW	l_1	15.0	1.50
003	UW	l_1	15.0	1.00
004	UW	l_1	15.0	2.00
005	UW	l_1	12.0	1.50
006	UW	l_1	12.0	1.00
007	UW	l_1	12.0	2.00
008	UW	l_1	20.0	1.50
009	UW	l_1	20.0	1.00
010	UW	l_1	20.0	2.00
011	UW	l_2	15.0	1.50
012	UW	l_2	15.0	1.00
013	UW	l_2	15.0	2.00
014	UW	l_2	12.0	1.50
015	UW	l_2	12.0	1.00
016	UW	l_2	12.0	2.00
017	UW	l_2	20.0	1.50
018	UW	l_2	20.0	1.00
019	UW	l_2	20.0	2.00

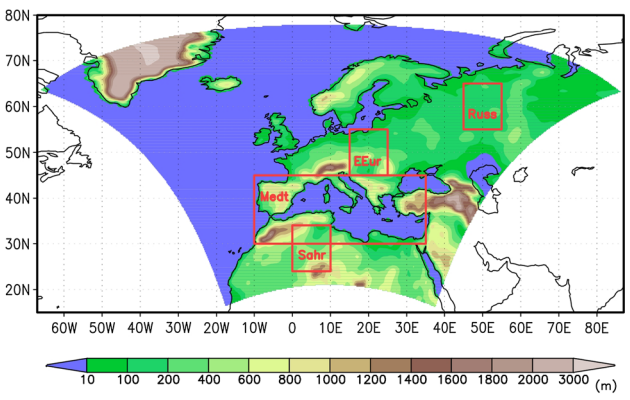

Fig. 1 The model domain, orography field (m) and selected regions (*Russ* Russia, *EEur* Eastern Europe, *Sahr* Sahara, *Medt* Mediterranean) for the vertical profile and ensemble sensitivity analysis

[3] Climatic Research Unit, University of East Anglia, Norwich, UK.

[4] Available from http://gforge.ictp.it/gf/project/regcm/.

Holtslag and Boville 1993) and the UW scheme (Grenier and Bretherton 2001; O'Brien et al. 2012). While the Holtslag scheme is used only inside the PBL with a different approach to vertical mixing applied above the PBL, the UW scheme utilizes a consistent mixing approach for all turbulent layers across the whole atmospheric column. In the following a short overview of the two PBL schemes is given and the ensemble of simulations is described.

2.1 The Holtslag PBL scheme

The temperature tendency due to vertical turbulent mixing is computed in RegCM as:

$$\left(\frac{\partial p^* T}{\partial t}\right)_{PBL} = p^* \frac{\partial}{\partial z}\left(K_H\left(\frac{\partial \theta}{\partial z} - \gamma\right)\frac{\Pi}{c_p}\right), \quad (1)$$

where $p^* = p_{SURF} - p_{TOP}$ represents the difference between surface pressure and pressure at the model top, T is air temperature, θ is potential temperature, K_H is eddy heat diffusivity, γ is a counter-gradient term that parameterises the dry deep-convection transport, Π is the Exner function and c_p is specific heat capacity of dry air at constant pressure. The counter-gradient term (see Eq. 3 below) parameterises the vertical heat transport due to large PBL eddies (e.g. Holtslag et al. 1990; Holtslag and Moeng 1991). Similar expressions for tendencies due to turbulent mixing are implemented in prognostic equations for wind components, and for water vapour and cloud water mixing ratios. However, the counter-gradient contribution is included only in the temperature prognostic equation. The Holtslag scheme is written in terms of potential air temperature, so the Exner function must be included in order to reconstruct air temperature.

In the Holtslag scheme, K_H inside the PBL is determined as:

$$K_H = k w_t z\left(1 - \frac{z}{h}\right)^2, \quad (2)$$

where $k = 0.4$ is the von Kármán constant, w_t is the turbulent velocity scale, z is the height inside PBL and h is the PBL height determined as the height where the gradient Richardson number Ri equals its critical value $Ri_C = 0.25$. It is assumed in the Holtslag scheme that the PBL mixing is forced only from the surface fluxes; otherwise, the whole concept of the Ri_C can be questioned (e.g. Mauritsen et al. 2007; Baklanov et al. 2011). The counter-gradient term γ is applied only in convective PBL layers (not in surface layer and not above PBL) and is determined as:

$$\gamma = C\frac{\left(\overline{w'\theta'}\right)_{SURF}}{w_t h}, \quad (3)$$

where $\left(\overline{w'\theta'}\right)_{SURF}$ is the surface heat flux (in kinematic units) and $C = 8.5$ (Holtslag et al. 1990).

Above the PBL, K_H is determined as a function of Ri, wind shear and the asymptotic turbulent length scale is set to $l_\infty = 40$ m (e.g. Pielke 2002):

$$K_H = K_{HO} + [Ri(\sigma) - Ri_C(\sigma)] \cdot l_\infty^2 \cdot \sqrt{\left(\frac{\Delta u}{\Delta z}\right)^2 + \left(\frac{\Delta v}{\Delta z}\right)^2}, \quad (4)$$

where σ is the model sigma vertical coordinate and K_{HO} is the background minimum vertical mixing coefficient. There are uncertainties related to the value of C in Eq. (3) (e.g. in Troen and Mahrt (1986) this parameter is set to $C = 6.5$). Also, there is no unique formulation or value of the asymptotic length scale l_∞ (Eq. 4) for vertical mixing above the PBL (e.g. Pielke 2002) which makes this parameter a candidate for sensitivity tests. However, since our focus is on the new PBL scheme in the RegCM model (the UW scheme), sensitivity experiments are primarily designed to examine the impact of the unconstrained parameters in the UW scheme.

In the Holtslag scheme, the maximum eddy diffusivity and viscosity are not constrained inside the PBL and are set to $0.8\Delta z^2/\Delta t$ above the PBL, where Δz is the layer depth and Δt is the model time step. At the same time, the minimum eddy diffusivity and viscosity are set to a relatively high value of 1 m^2 s^{-1} inside and above the PBL. However, for very stable conditions, eddy heat diffusivity and viscosity are set to 0 m^2 s^{-1}; this was shown to reduce a part of the warm bias during winter in the high latitude regions (Güttler 2011).

2.2 The UW PBL scheme

Whereas in the Holtslag scheme the origin of turbulent mixing is surface heating due to incoming solar radiation and related static instability, the UW scheme considers also a second region of the increased turbulent activity and mixing which is associated with the buoyancy perturbations due to the cloud-top entrainment instability and longwave cooling present at e.g. the stratocumulus-topped PBLs (e.g. Stull 1988). Of course, both schemes "sense" turbulent mixing due to surface friction and wind shear. The UW scheme is developed in terms of liquid water potential temperature and total water mixing ratio and a separate iterative reconstruction determines PBL tendencies for air temperature and for water vapour and cloud water mixing ratios. In the UW scheme, the eddy heat diffusivity K_H is related to the turbulent kinetic energy (TKE) following Mellor and Yamada (1982):

$$K_H = l\sqrt{2 \cdot TKE} \cdot S_H, \quad (5)$$

where S_H is the stability function (e.g. Galperin et al. 1988) and l is the master turbulent length scale with two options

implemented in RegCM. In convective boundary layers, one of the two following formulations for l can be chosen in initial model setup:

$$l_1 = \frac{\min(\mathrm{kz}, 0.1\,\Delta z)}{1 + \frac{\min(\mathrm{kz}, 0.1\,\Delta z)}{\lambda}}, \tag{6}$$

$$l_2 = \min(kz, 0.1\,\Delta z), \tag{7}$$

where l_1 is based on Blackadar (1962) and l_2 is consistent with the fact that in layers close to the surface, the distance from surface limits the size of turbulent eddies (e.g. Stull 1988); λ is the asymptotic master turbulent length scale set to $0.085\Delta z$, where Δz is the depth of the convective sublayer (Grenier and Bretherton 2001). For the same z and Δz, l_2 is larger than l_1 and the use of l_2 increases eddy heat diffusivity K_H (cf. Eq. 5). In stably stratified conditions, there is no difference in the formulation of the master length, i.e.

$$l_1 = l_2 = \min\left(R_{STBL}\sqrt{\frac{TKE}{N^2}}, kz\right), \tag{8}$$

where N is buoyancy (or the Brunt-Väisälä) frequency and R_{STBL} is a scaling factor [e.g. Nieuwstadt 1984; see Mahrt and Vickers (2003) and Grisogono (2010) for the discussion]. Only at the top of the cloud-topped PBL the following closure for the eddy heat diffusivity is assumed (Nicholls and Turton 1986):

$$K_H = w_e \Delta_i z, \tag{9}$$

where w_e is the entrainment rate determined as

$$w_e = A\frac{TKE^{3/2}}{l\Delta_i b}, \tag{10}$$

$$A = a_1(1 + a_2 E), \tag{11}$$

where A is the entrainment efficiency, $\Delta_i b$ is the buoyancy difference across $\Delta_i z$ (the depth of the entrainment layer), a_1 is based on observations and set to 0.19, E parameterises the evaporative enhancement of entrainment efficiency (e.g. Grenier and Bretherton 2001; their Appendix B) and a_2 is largely unconstrained parameter ranging from 10 to 100 [see e.g. Bretherton and Park (2009) for the discussion of the range of the a_2 parameter].

As a part of the UW scheme, an additional prognostic equation for TKE is implemented where the local change of TKE is governed by buoyancy production and destruction, shear production, turbulent vertical transport and turbulent dissipation (e.g. Grenier and Bretherton 2001). Additionally, the RegCM dynamical core computes the TKE horizontal and vertical advection and horizontal diffusion (second, third and last terms in the following equation):

$$\frac{\partial TKE}{\partial t} + \vec{u}\cdot\vec{\nabla}TKE + w\frac{\partial TKE}{\partial z} = -K_H N^2 + K_M S_f^2 + \frac{\partial}{\partial z}\left(K_{TKE}\frac{\partial TKE}{\partial z}\right) - B_1\frac{TKE^{3/2}}{l} + D, \tag{12}$$

where K_M and K_{TKE} are the momentum and TKE turbulent diffusivities respectively, S_f^2 is the wind shear squared, B_1 is a constant in the turbulent dissipation term and D is horizontal diffusion term. In the RegCM implementation of Eq. 12, vertical gradient and vertical velocity are transformed to the σ vertical coordinate system. The inclusion of the TKE prognostic equation increases the RegCM computational requirements only moderately (e.g. simulations with the UW scheme take approximately 30 % more computer time when compared to simulations with the Holtslag scheme).

In the UW PBL scheme the minimum eddy heat diffusivity is not directly fixed, but a lower limit of 10^{-8} m^2 s^{-2} is used for TKE. The maximum eddy heat diffusivity K_H is set to 10^4 m^2 s^{-1}. Although the different upper and lower limits of the eddy heat diffusivity (and TKE) in the Holtslag and the UW PBL schemes reflect their separate development, they are present in the RegCM model primarily to ensure computational stability. Their implementation should be revisited in future model development and tested for cases of statically very stable and unstable conditions, i.e. to explore relative importance of lower and upper limits on K_H respectively.

2.3 Perturbed physics ensemble

Sensitivity of model climatology to several important aspects of the UW scheme was tested in an ensemble of RegCM simulations. Different formulations of the master turbulent scale l (Eqs. 6, 7) and the values of a_2 (Eq. 11) and R_{STBL} (Eq. 8) are systematically varied (Table 1) producing an 18-member ensemble. The parameter a_2 can be interpreted as the efficiency of evaporative enhancement of the cloud-top entrainment. In the region of mixing of the cloud-top air and the above-inversion air, evaporative cooling may force further sinking of the mixed air thus resulting in enhanced entrainment (Bretherton and Park 2009). A reduced a_2 means that "for a given TKE, higher cloud-top liquid water content (a thicker cloud) is needed to generate a given entrainment rate" (Grenier and Bretherton 2001). As a consequence, the reduction of a_2 can locally reduce the magnitude of eddy diffusivity (cf. Eqs. 9–11) and modify the vertical slope of the eddy diffusivity profile thus directly impacting temperature tendency from the PBL scheme (cf. Eq. 1). Knight et al. (2007) emphasized the importance of the entrainment rate which was associated with a 30 % variability of climate

sensitivity in their large PPE. Both, the importance of entrainment in large PPE and limitations in measuring its effects, make the parameter a_2 a prime candidate to test in a model environment.

Changes in the formulation of the l and R_{STBL} parameters can have similar impacts as changes in a_2. We hypothesize that a reduction of the vertical mixing and temperature tendencies from the PBL scheme will result from the reduction of any of these parameters (cf. Eqs. 5–8). The choice and formulation of l, especially in stably stratified PBL, is an open topic in atmospheric turbulence (e.g. Grisogono 2010) and in RegCM only the simplest formulations are implemented. The master turbulent length scale formulations in PBL schemes should be explored in the future RegCM model development since other elements in the Eq. (5) are already strongly constrained by both theory and observations.

Within the context of the present formulation of l in the UW scheme, the experiments in Table 1 are broadly divided in two subsets: one when l is formulated as in Eq. (6), and one when l is formulated as in Eq. (7). For each definition, l_1 or l_2, in addition to the default value (15.0), the parameter a_2 is varied so as to acquire a value larger than the default and a value smaller than the default ($a_2 = 20.0$ and $a_2 = 12.0$, respectively). Similarly, for each value of a_2, the parameter R_{STBL} is varied around its default value (1.5) with smaller and larger values relative to the default ($R_{STBL} = 1.0$ and $R_{STBL} = 2.0$, respectively). In such a way, the changes in the UW parameters considered are nearly "symmetrical" relative to their default values; the aim is to assess their possible impacts when it is not a priori clear what might be the ultimate model response to such changes.

3 Seasonal T2m and precipitation errors in two PBL schemes

The RegCM experiments with different PBL schemes discussed in this study substantially differ in *T2m* climatology but less so in precipitation climatology. The use of the UW scheme is mostly beneficial and in the following we identify possible mechanisms that could be responsible for detected differences. In this section, the model systematic errors in *T2m* and precipitation in experiments with two PBL schemes are compared. In the following section, vertical profiles of air temperature and water vapour mixing ratio (both being prognostic variables in RegCM and closely related to the near-surface temperature and precipitation) over four selected regions are compared. Next, the eddy heat diffusivity and tendencies in temperature and water vapour mixing ratio due to different PBL schemes are analyzed, whereas in Supplement 2 evaluation of sensible and latent heat fluxes over four selected regions is provided. Finally, the amplitude and variability of *T2m*, specific humidity at 2 m *q2m* and eddy heat diffusivity K_H at the first model level are explored in an ensemble of the UW simulations.

The reference simulation using the Holtslag scheme, denoted as EXP001 (Table 1), reveals an underestimation of *T2m* relative to CRU data over the northern Africa during DJF, with errors typically between −2 and −4 °C (Fig. 2a). *T2m* in the central parts of the domain is simulated well with the mean errors between −1 and 1 °C. In the northern and north-eastern parts of the domain, the RegCM simulation with the Holtslag PBL scheme overestimates *T2m*, typically between 2 and 4 °C. In the previous version of RegCM even larger *T2m* overestimation was observed over the same region and it was linked with model deficiencies in simulating very cold and stable conditions associated with increased cloudiness (Güttler 2011). The warm bias in the RegCM winter simulations is also seen over other domains, e.g. North America (Mearns et al. 2012) and Asia (Ozturk et al. 2012). Large *T2m* systematic errors are also found during JJA in the central part of the European domain, ranging between 2 and 4 °C (Fig. 2c). We explore below whether the *T2m* systematic errors seen in Fig. 2a, c can be reduced when the UW scheme is used in RegCM; in Vautard et al. (2013) and Güttler et al. (2013) some other possible sources of these systematic errors are suggested.

The spatial distribution of the *T2m* JJA errors differs from that in DJF, pointing to a possibly different origin of these errors in two contrasting seasons. Coppola et al. (2012) detected similar spatial structure of the *T2m* errors (their Fig. 8) in the, so-called, tropical-band version of RegCM (where RegCM is limited only by the southern and northern boundaries). They also reported the cold bias over the Sahara desert during DJF, but the cold bias dominated in JJA over the western Sahara and the warm bias over the eastern Sahara. This suggests that some local processes are possible sources of *T2m* errors over the northern Africa, because in Coppola et al. (2012) the upper-air flow over northern Africa was not influenced by the nesting and by domain size.

The *T2m* response in our UW experiment (EXP002), where all other aspects of the model parameterisations were retained unchanged, is shown in Fig. 2b, d. The JJA *T2m* errors relative to CRU are now generally reduced, with magnitude between 1 and 2 °C (Fig. 2d). However, in the winter, the cold bias over the northern Africa is enhanced with the UW scheme, thus contributing to an increase of the overall mean error (computed over the entire domain) from −0.02 °C in the Holtslag scheme to −1.02 °C in the UW scheme. A similar model response was documented also by O'Brien et al. (2012) in their

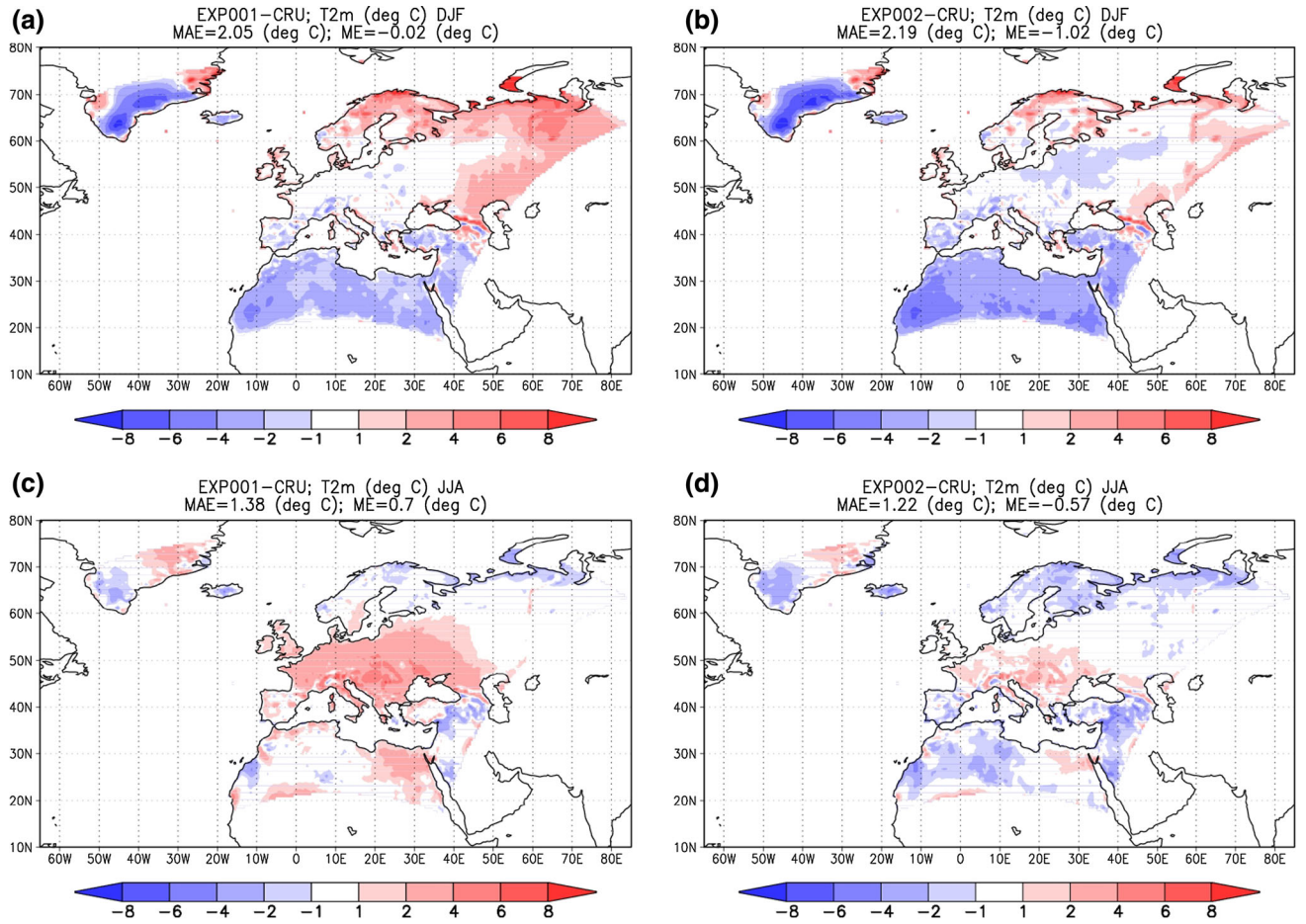

Fig. 2 The air temperature at 2 m (*T2m*) systematic errors in EXP001 (with the Holtslag PBL scheme; *left*) and EXP002 (with the UW PBL scheme; *right*) when compared against CRU TS 3.0. Winter *errors* are shown in *top panels* and summer *errors* are shown in *bottom panels*. The period simulated is 1989–1998. MAE (mean absolute error) and ME (mean error) are computed over the entire domain. Units are °C

simulations over the North American region. A possible origin of such a cooling induced by the UW scheme will be explored in the subsequent sections by analyzing vertical profiles of eddy heat diffusivity and temperature tendency. Nevertheless, we can judge that, in terms of *T2m* climatology, the use of the UW scheme in EXP002 is beneficial over the domain considered in spite of somewhat increased cold bias over the northern Africa during the winter. Potential sources of the near-surface temperature bias over the northern Africa can include the limitations and/or deficiencies in the albedo specification in the land-surface scheme (Sylla et al. 2010), the overestimation of the total cloud cover over this region during DJF (Güttler et al. 2013) and the need to include the aerosol-related processes in RegCM simulations (Solmon et al. 2012). However, the RegCM simulations of surface and near-surface climatology over the whole Africa is comparable to other regional climate models (e.g. Kothe and Ahrens 2010; Kim et al. 2013).

The experiment including the UW scheme (EXP002) is wetter than the default experiment EXP001; this is seen in the mean seasonal precipitation when compared against CRU (Fig. 3). Already present in EXP001, the wet winter bias, with the magnitude between 0.5 and 1 mm day^{-1} (Fig. 3a), is slightly increased in EXP002 (Fig. 3b). However, the precipitation increase has a positive impact on summer climatology. Here, the dry bias over central Europe is much reduced in EXP002 (cf. Fig. 3c, d), but it still persists in the south-eastern Europe. As an important side note, it is obvious from Fig. 3 that the coastal/mountainous regions are most prone to systematic precipitation errors in RegCM, possibly indicating the need of using the higher horizontal resolutions in order to reduce errors associated with under-resolved orographic enhancement of precipitation.

4 Vertical profiles

In Fig. 1 four selected regions are shown within the model domain, representing various climatic regimes, where

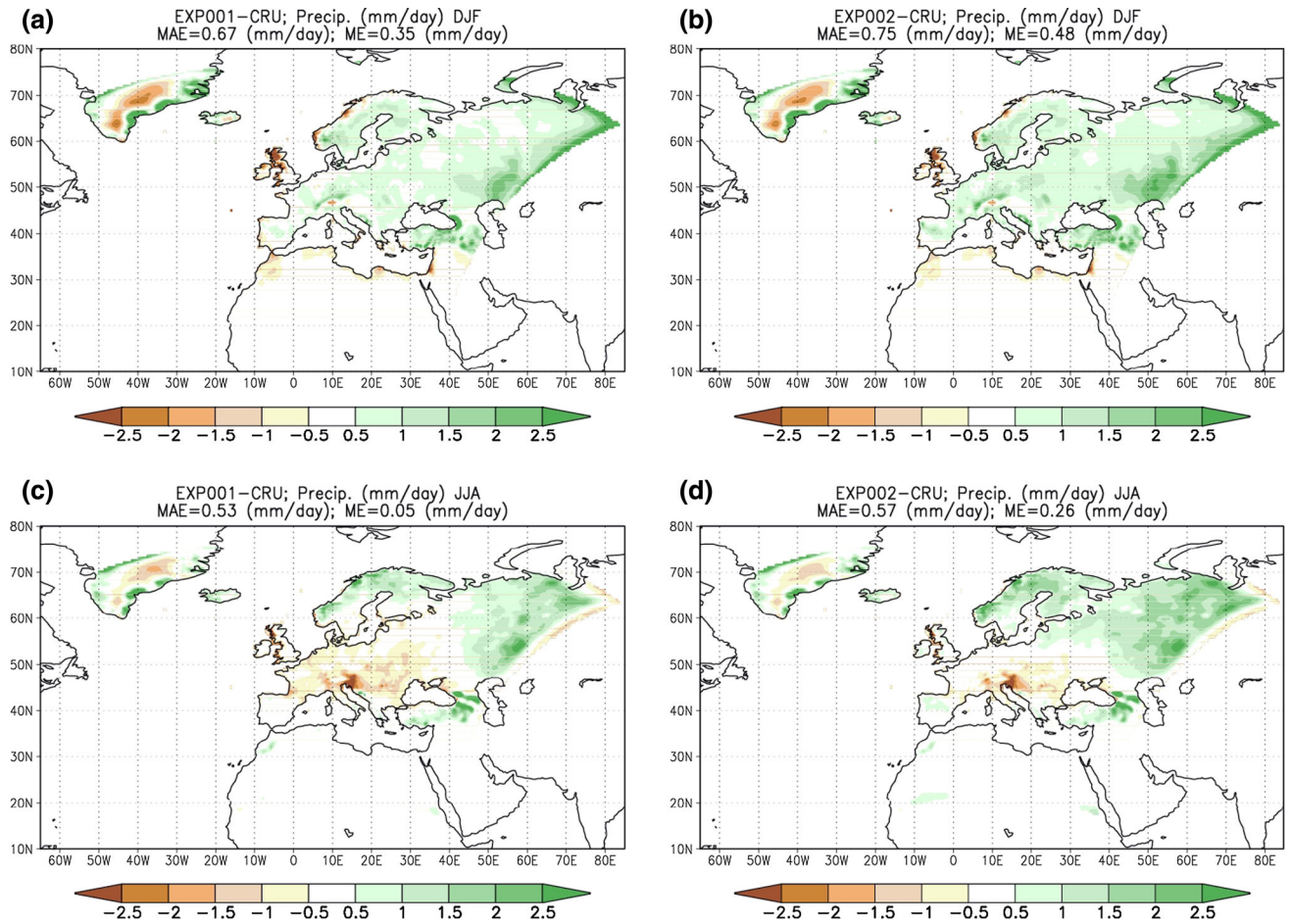

Fig. 3 Same as Fig. 2 but for precipitation. Units are mm day^{-1}

model sensitivity to different PBL scheme could be distinctly manifested: Russia (45–55°E, 55–65°N) is characterized by low temperatures with persistent snow cover during winter and early spring with frequent formation of shallow and very stable PBLs; Eastern Europe (15–25°E, 45–55°N) covers a typical European continental region; Sahara (0–10°E, 24–34°N) is defined over the desert area in the North Africa, where strong daytime turbulent mixing is present during the whole year; Mediterranean (−10°W to 35°E, 30–45°N) is partially overlapping with the region Sahara and in a large part of the domain atmospheric processes are influenced by the sea. The analysis is focused on the area means over land points because the CRU data are available over land only. The differences between the two schemes shown and discussed for the averages over land points in the Mediterranean region are generally similar to the averages over sea points (Fig. S1).

Our analysis can be viewed as a comparison of the non-local and local PBL schemes in the full model framework. On the other hand, the study by Bretherton and Park (2009) is a comparison of the non-local and local schemes (i.e. schemes similar to those as in our study) in a controlled 1-D framework where three types of PBLs are simulated and compared against large eddy simulations and observations: (1) dry convective boundary layer; (2) stably stratified boundary layer; (3) nocturnal stratocumulus-topped boundary layer. In (1) both schemes performed equally well in general; in (2) the local scheme was modified by reducing the free-troposphere mixing length and thus made comparable to the non-local scheme; in (3) the non-local scheme (similar to the UW scheme) performed much better because of the inclusion of the entrainment effects at the top of the cloud-topped PBL.

4.1 Air temperature and water vapour mixing ratio

The mean winter and summer vertical profiles of the air temperature (T) over four selected regions in the Holtslag scheme (EXP001) are presented in Fig. 4a, b and the impact of the UW scheme is shown in terms of differences between EXP002 and EXP001 (Fig. 4c, d). Figure 4a, b clearly indicates the impact of regional geophysical properties on temperature profiles: with Russia being the coldest and Sahara the warmest region in both seasons. The

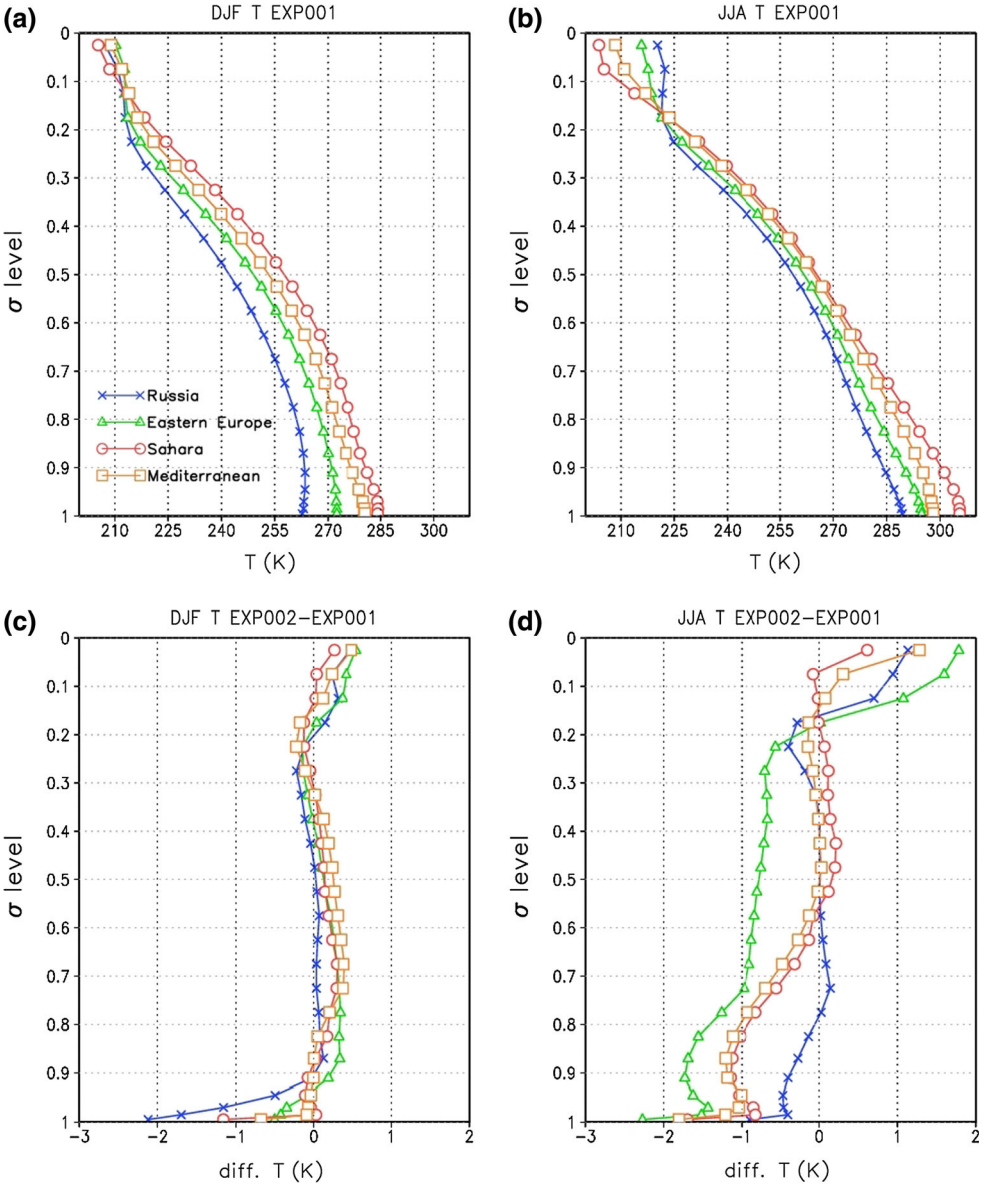

Fig. 4 Vertical profiles of the regional- and seasonal-mean air temperature *T* in EXP001 (the Holtslag PBL scheme; *top*) and the difference between EXP002 (the UW scheme) and EXP001 (*bottom*). Winter profiles are in the *left*-hand column, summer profiles are in the *right*-hand column. The period analyzed is 1989–1998 and selected regions are shown in Fig. 1. Profiles over Russia are marked by *crosses*, over Eastern Europe by *triangles*, over Sahara by *circles* and over Mediterranean by *squares*. Units are K

differences between the PBL schemes (Fig. 4c, d) are in general larger during JJA (cooling with the UW scheme between 1 and 2 °C) than during DJF (cooling between 0 and 1 °C) and are mostly found at the model low levels, although the differences of the opposite sign are seen at the stratospheric levels as well (up to 2 °C over Eastern Europe). Figure 4c, d indicates a significant sensitivity of the model results to the choice of PBL scheme and an impact on temperature profiles, particularly in the regions and at atmospheric layers where turbulent mixing is important. For example, during summer, when turbulent mixing due to solar heating of the surface is strongly active in the lowest model layers, a prominent cooling with the UW scheme takes place in all regions except Russia. In contrast, during DJF, the strongest cooling is found over the Russian region at the lowest levels. As seen in the previous section, this is consistent with the improvements in the *T2m* climatology when compared against CRU data over this region.

For water vapour mixing ratio (*qv*), Fig. 5a shows that in winter, Russia is much drier than Sahara (at the same time, cloud water mixing ratio is higher over Russia; not shown), but in summer (Fig. 5b) there is little difference among the regions except Sahara. The mean differences between the UW scheme (EXP002) and the Holtslag scheme (EXP001) indicate an increase of *qv* at the model lowest levels and a decrease around $\sigma = 0.7$ during JJA (Fig. 5d). During DJF, the *qv* profiles show a decrease over Russia and an increase over all other three regions when the UW scheme is used. Again, model sensitivity to the UW PBL scheme is most

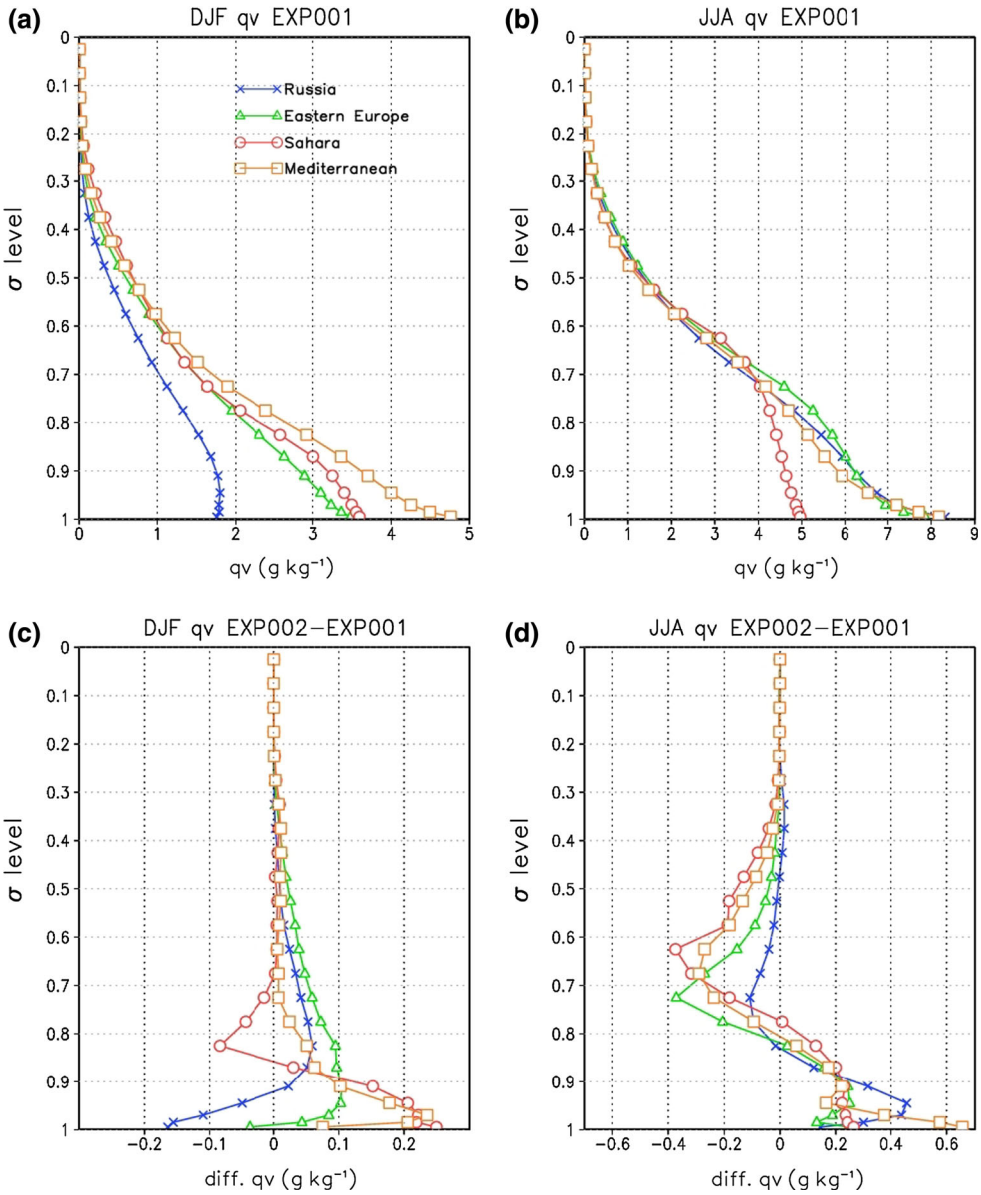

Fig. 5 Same as Fig. 4 but for water vapour mixing ratio *qv*. Units are g kg^{-1}

expressed during JJA with the largest increase at the lowest model levels of up to 0.6 g kg^{-1} over Mediterranean and a decrease of up to 0.4 g kg^{-1} in the mid-tropospheric layers in Eastern Europe and Sahara. The moistening of the lower atmosphere over Russia and Eastern Europe (Fig. 5c, d) is consistent with the increased precipitation amounts when the UW scheme is employed (Fig. 3b, d). Differences between the two schemes are also seen in the cloud-related variables: cloud water mixing ratio and cloud fraction. While the differences in the cloud water mixing ratio are highly variable in space (i.e. over different regions) and seasons, the cloud fraction in EXP002 is increased relative to EXP001 at each vertical layer in all four regions and in both seasons (not shown). This is consistent with the lower temperatures (Fig. 2b, d) and the higher relative humidity in the UW experiment and supports the relationship between underestimated cloud cover and overestimated surface net shortwave radiation flux and surface temperature in experiments using the Holtslag scheme (Güttler et al. 2013).

We note here that the current implementation of the Holtslag scheme in RegCM does not include the contribution of the counter-gradient term to the calculation of tendencies in prognostic equation for water vapour mixing ratio. This is a variation from the original Holtslag et al. (1990) formulation and was implemented in RegCM by Giorgi et al. (2012) in order to reduce too dry conditions in the lower atmosphere. This modification in the Holtslag scheme simplifies its comparison with the UW scheme since, by design, in the UW scheme no counter-gradient term is included.

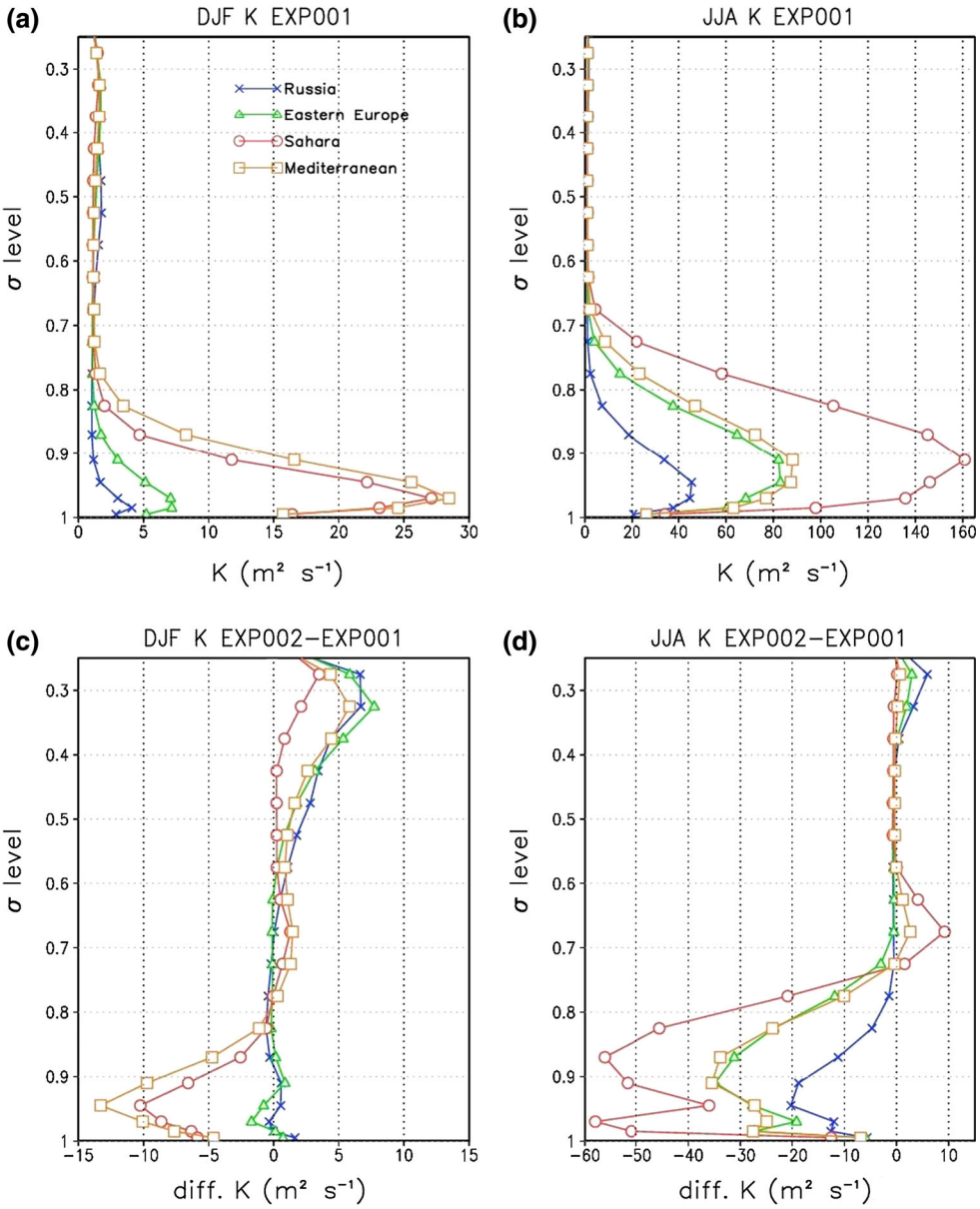

Fig. 6 Same as Fig. 4 but for the eddy heat diffusivity K_H and $\sigma = [1.0, 0.25]$. Units are $m^2\ s^{-1}$

4.2 Eddy heat diffusivity

Vertical profiles of eddy heat diffusivity[5] K_H in the default EXP001 experiment include the maximum in the lower atmosphere (around $\sigma = 0.9$) with the mean JJA magnitude of up to 160 $m^2\ s^{-1}$ over the Sahara region, and between 40 and 90 $m^2\ s^{-1}$ in other regions (Fig. 6a, b). Even higher values of K_H are documented in Giorgi et al. (1993) but these included monthly means for specific hourly profiles (e.g. monthly means of all vertical profiles at 12 UTC). The magnitude of the winter K_H maximum in Fig. 6a is between 5 and 30 $m^2\ s^{-1}$ and it decreases from south to north. The eddy heat diffusivity profiles over the Mediterranean region are in DJF similar to the profiles over Sahara (Fig. 6a, c) and in JJA to the profiles over the Eastern Europe (Fig. 6b, d). For the winter, this may partially reflect the impact of sea surface temperature (SST) on turbulent mixing on the nearby coastal land areas because in the Mediterranean region land points are intermingled with sea points: higher SST during DJF is consistent with more instability possibly influencing the surrounding land. In summer, the sea is cooler than surrounding land and the eddy heat diffusivity is much lower than over hot Sahara region.

Similar to air temperature and water vapour mixing ratio, the differences in K_H between the experiments with two PBL schemes are mainly in the lower atmosphere with

[5] From now on, all vertical profiles are shown for the σ interval [1.0, 0.25], where the main differences between two PBL schemes occur.

the JJA differences larger than those during DJF (Fig. 6c, d). The UW scheme is less diffusive (i.e. the differences are predominantly negative) indicating less vertical turbulent mixing than in the Holtslag scheme, with the differences of up to 60 $m^2\ s^{-1}$ over the Sahara in JJA and between 20 and 40 $m^2\ s^{-1}$ over other regions. This is consistent with the result of Cuxart et al. (2006) who found, for a moderately stably stratified PBL, a general reduction of turbulent mixing in prognostic schemes when compared to diagnostic schemes. Additionally, a secondary layer with a slightly increased eddy turbulent diffusivity in EXP002 is present near $\sigma = 0.3$ ($\sim$330 hPa). These increased values of K_H at the high altitudes in Russia and Eastern Europe during DJF (Fig. 6c) can be associated with the shear-induced mixing in the UW scheme near the jet stream regions. A double-peak structure in the K_H differences, seen in Fig. 6d, between $\sigma = 1.0$ and $\sigma = 0.9$ during JJA over Eastern Europe and Sahara (and less obvious over Russia and Mediterranean) is the consequence of a slightly lower positioning of the K_H maximum in the UW scheme and a sharper increase of the K_H from the surface upwards.

By ignoring the counter-gradient term and rewriting it in a simplified form, i.e. only in terms of air temperature T, Eq. (1) can be converted into

$$\frac{\partial T}{\partial t} = \frac{\partial}{\partial z}\left(K_H \frac{\partial T}{\partial z}\right) = K_H \frac{\partial^2 T}{\partial z^2} + \frac{\partial K_H}{\partial z}\frac{\partial T}{\partial z}. \qquad (13)$$

From Eq. (13) it is clear that both the magnitude of K_H (always positive; Fig. 6a, b) and the slope $\partial K_H/\partial z$ (positive below and negative above the maximum at levels between $\sigma = 1.0$ and $\sigma = 0.9$), in interaction with the curvature ($\partial^2 T/\partial z^2$) and the slope ($\partial T/\partial z$) of the air temperature vertical profiles respectively, govern the sign and the magnitude of the temperature tendencies from the PBL scheme.[6] Obviously, the K_H profile in the UW scheme is different to that of the Holtslag scheme: its magnitude and slope are generally reduced (Fig. 6c, d). A simplification similar to Eq. (13) and the corresponding discussion of vertical profiles holds also for the water vapour mixing ratio. The ultimate impact to the vertical profile of any prognostic variable depends on additional interactions between the PBL scheme and all other model components, so different signs of temperature tendency and different signs of the T and qv differences between EXP001 and EXP002 are also possible.

[6] Although no simple physical interpretation of changes in turbulent eddy characteristics is obvious when changing the slope or curvature of temperature profile, one can note a "diffusion-like" ($\partial T/\partial t = K_H \partial^2 T/\partial z^2$) and a "wave-like" ($\partial T/\partial t = \partial K_H/\partial z\ \partial T/\partial z$; where units of $\partial K_H/\partial z$ are ms^{-1}) parts of Eq. 13.

4.3 Temperature and water vapour tendencies

The general structure of the RegCM vertical profiles of the total temperature tendency from the Holtslag PBL scheme, shown in Fig. 7a, b (where temperature tendencies are split into total and counter-gradient terms), is comparable to that in Giorgi et al. (1993; their Fig. 6a), though the different temporal and spatial scales are analyzed here. It is governed by the eddy heat diffusivity profile: temperature tendency is the highest at lower levels where K_H slope is substantial (cf. Fig. 6a, b in conjunction with the last term $\partial K_H/\partial z\ \partial T/\partial z$ in Eq. 13). At levels with the maximum K_H, where the contribution of the K_H slope is negligible ($\partial K_H/\partial z \approx 0$), temperature tendency is still positive, implying that the air temperature curvature contribution (i.e. $K_H \partial^2 T/\partial z^2$; Eq. 13) is positive and dominant. Because of vertical mixing within PBL, heat from the surface is being transferred upwards (see Supplement 2) and warms the lower atmosphere, corresponding to a universally positive temperature tendency in Fig. 7a, b. The magnitude of the (positive) temperature tendency is decreasing with height and becomes negligible around $\sigma = 0.7$ ($\sim$700 hPa; cf. Fig. S2 for the air temperature tendencies due to the PBL zoomed to the lowest levels $\sigma = [1.0, 0.7]$). The total PBL temperature tendencies over Russia, Eastern Europe and Mediterranean during the winter are weaker than in summer due to a weaker insolation. However, over Sahara, where solar heating generates and supports turbulent mixing essentially throughout the year, the winter and summer PBL temperature tendencies are of comparable magnitude.

The contribution of the counter-gradient term (shown in Fig. 7a, b by solid markers and the + marker) to the total PBL tendency is important in all regions during JJA, but also during DJF over Mediterranean and Sahara. The counter-gradient flux tends to reduce temperature tendency in the lower PBL and slightly warms the atmosphere around $\sigma = 0.8$ ($\sim$800 hPa). It is associated with the parameterised deep eddies which originate in the lower parts of the convective PBL and transfer heat to the upper (sometimes slightly stably stratified) layers (Holtslag et al. 1990; Holtslag and Moeng 1991). According to Fig. 7, this process occurs over the European continent in JJA and also over the arid northern Africa and parts of the southern Europe during DJF.

In both seasons and in most regions, the temperature tendency with the UW scheme is reduced at many model levels in the lower atmosphere (Fig. 7c, d). This reduction is up to 6×10^{-5} Ks^{-1} relative to the same tendency in the Holtslag scheme. Differences between the UW and Holtslag PBL temperature tendencies (Fig. 7c, d) reflect the changes in the eddy heat diffusivity profiles. For example, the reduced values of eddy heat diffusivity K_H in EXP002 (Fig. 6c, d) are associated with the reduction of the slope in

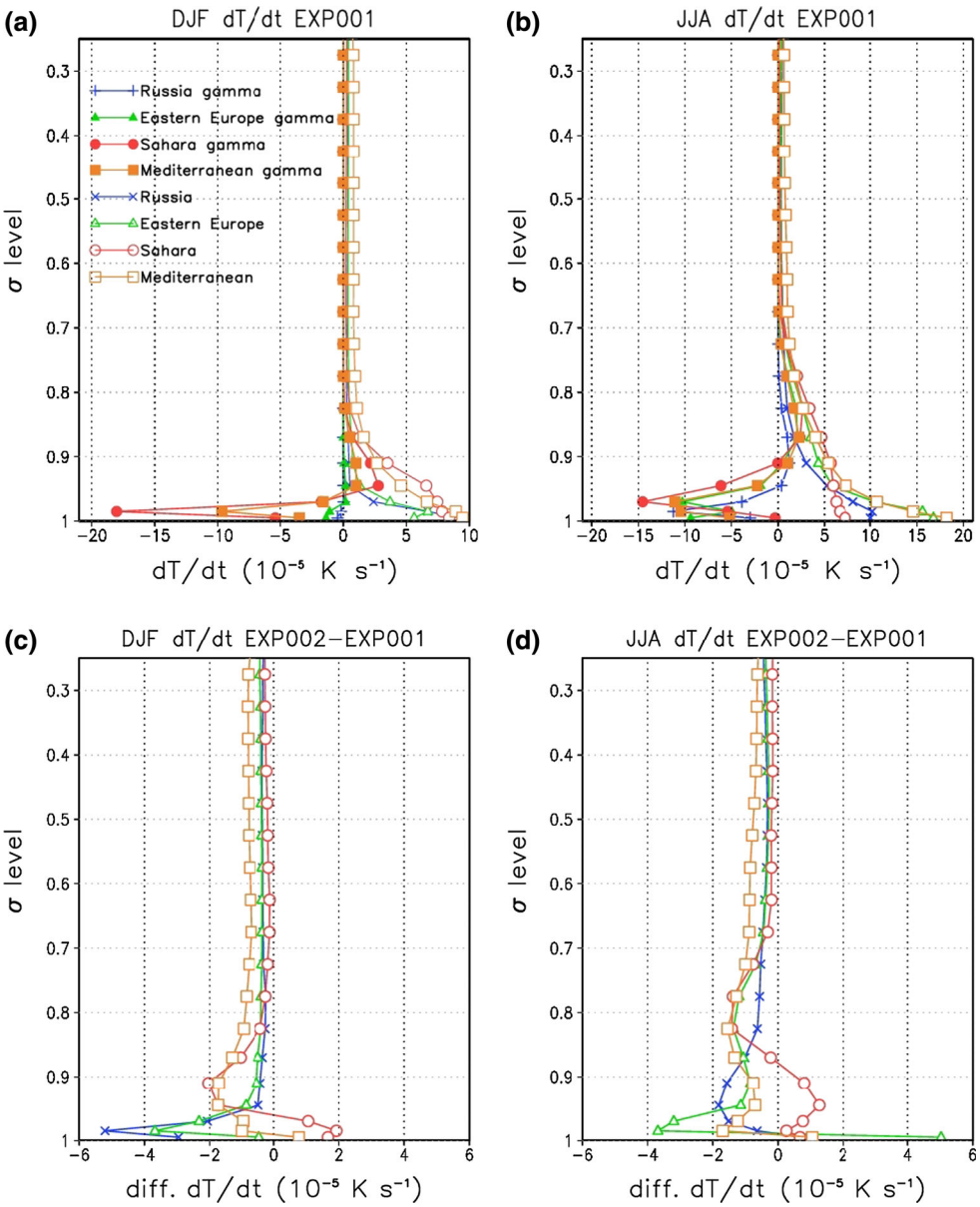

Fig. 7 Same as Fig. 4 but for the air temperature tendency due to the PBL scheme and $\sigma = [1.0, 0.25]$. Units are 10^{-5} Ks^{-1}. Additionally, the air temperature tendency in the Holtslag scheme due to counter-gradient contribution (Eq. 1) is shown in the *top row* (the + *marker* for Russia and *solid markers* for other regions)

the K_H vertical profile when compared to the default EXP001 run (cf. Eqs. 1, 13).

The (negative) sign of the PBL-generated temperature tendency differences is generally consistent with the cooling of PBL in the UW scheme seen in Fig. 4. However, the opposite to this dominant response is found at the first model level during JJA in all regions as well as at the first five levels during JJA and three lowermost levels in DJF over Sahara. Here, the UW scheme produces a higher temperature tendency than the Holtslag and the differences in Fig. 7c, d are positive. This is very likely the consequence of the inclusion of the counter-gradient flux in the Holtslag scheme which reduces the total temperature tendency, over the Mediterranean and Sahara regions (Fig. 7a, b, solid markers and the + marker).

The water vapour mixing-ratio (PBL-generated) tendencies due to the Holtslag scheme are positive in the bottom half of the atmospheric column in all four regions and in both seasons (Fig. 8a, b). Vertical structure and the order of magnitude of the tendencies shown in Fig. 8a, b are comparable to those from Giorgi et al. (1993). An analysis similar to that for temperature tendencies, based on Eq. (13), can be applied to the water vapour mixing-ratio (qv) tendencies. Vertical gradient $\partial qv/\partial z$ is always negative (i.e. qv decreases with height), implying that the curvature contribution $\partial^2 qv/\partial z^2$ (cf. Eq. 13) is dominant and produces the positive qv PBL tendency in the lowest levels. Over the Eastern Europe, the qv tendencies reach 50×10^{-6} g kg^{-1} s^{-1} in JJA (Fig. 8b) and 10×10^{-6} g kg^{-1} s^{-1} in DJF over Russia

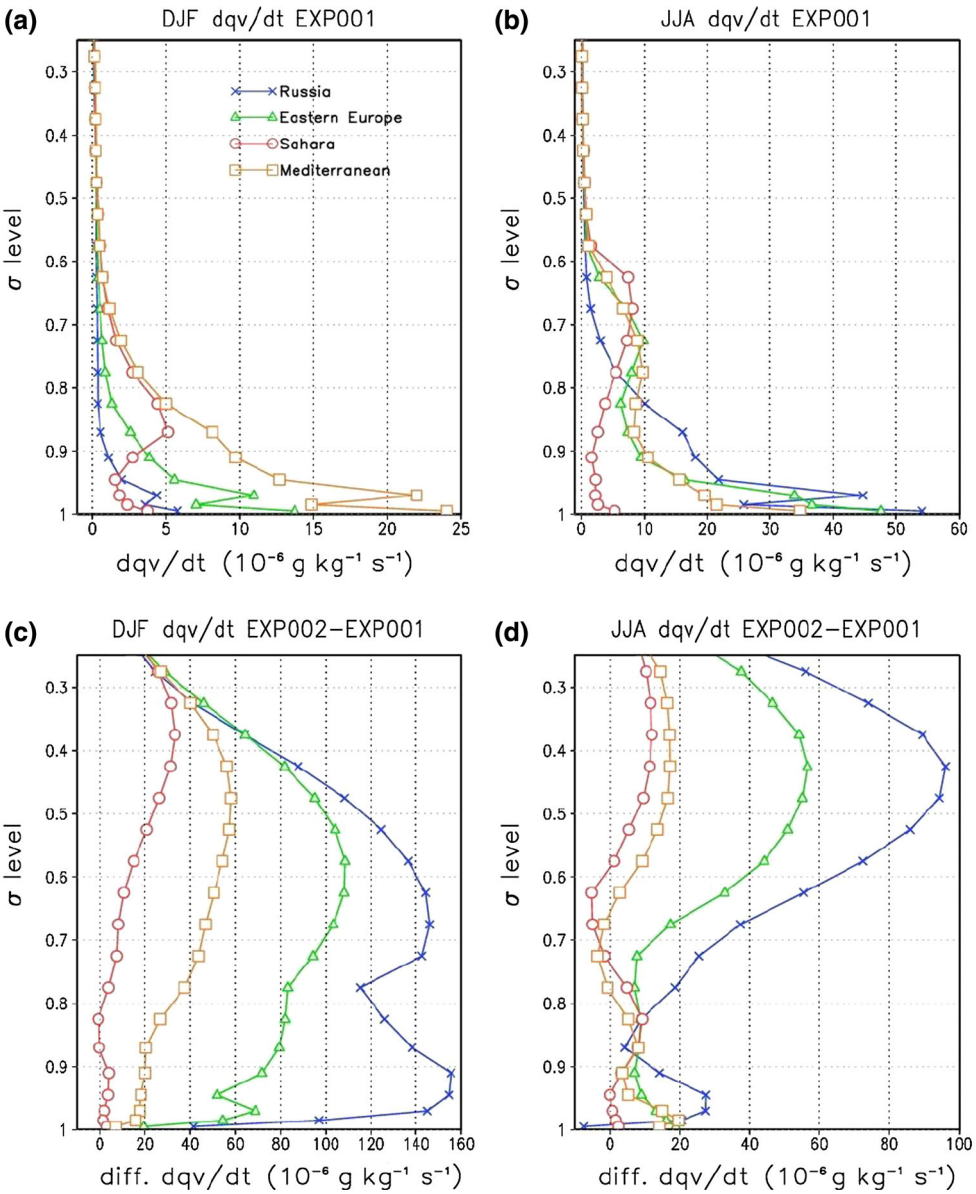

Fig. 8 Same as Fig. 4 but for water vapour tendency due to the PBL scheme and $\sigma = [1.0, 0.25]$. Units are 10^{-6} g kg^{-1} s^{-1}

and Eastern Europe respectively (Fig. 8a). In the southern regions, the magnitude of the *qv* tendencies is comparable in two extreme seasons and equals 5×10^{-6} g kg^{-1} s^{-1} over Sahara and around 30×10^{-6} g kg^{-1} s^{-1} over Mediterranean. However, an increase in the *qv* PBL tendency around $\sigma = 0.7$ in JJA and around $\sigma = 0.9$ in DJF is seen over Sahara (Fig. 8a, b). Since the PBL over Sahara is well mixed throughout the year, the tendency maximum at $\sigma = 0.7$ can be interpreted as a persistent loss of moisture from the PBL to the free atmosphere.

Of all the variables analyzed in this study, the most pronounced differences between simulations with different PBL schemes are seen for the *qv* tendencies (Fig. 8c, d). They include a major increase in the *qv* tendencies in almost the entire vertical column in EXP002, with largest differences during DJF[7] and over Russia and Eastern Europe. This increase is often up to the two orders of magnitude larger than that in the original EXP001 profiles (cf. Fig. 8a, b). The increase in the lower-atmospheric layers is consistent with the positive *qv* differences in the lower PBL, but it seems that some other indirect processes may have also contributed to the *qv* profile; for example, the *qv* vertical profile includes drying of PBL around $\sigma = 0.7$ (Fig. 5). Further research is needed to investigate possible contributions of some other parameterisations and/or resolved processes to temperature and water vapour mixing ratio tendencies (e.g. van de Berg et al. 2007).

[7] We recognize that these changes in *qv* tendency seem surprisingly large, however, we have rigorously verified that they reflect the actual PBL tendencies.

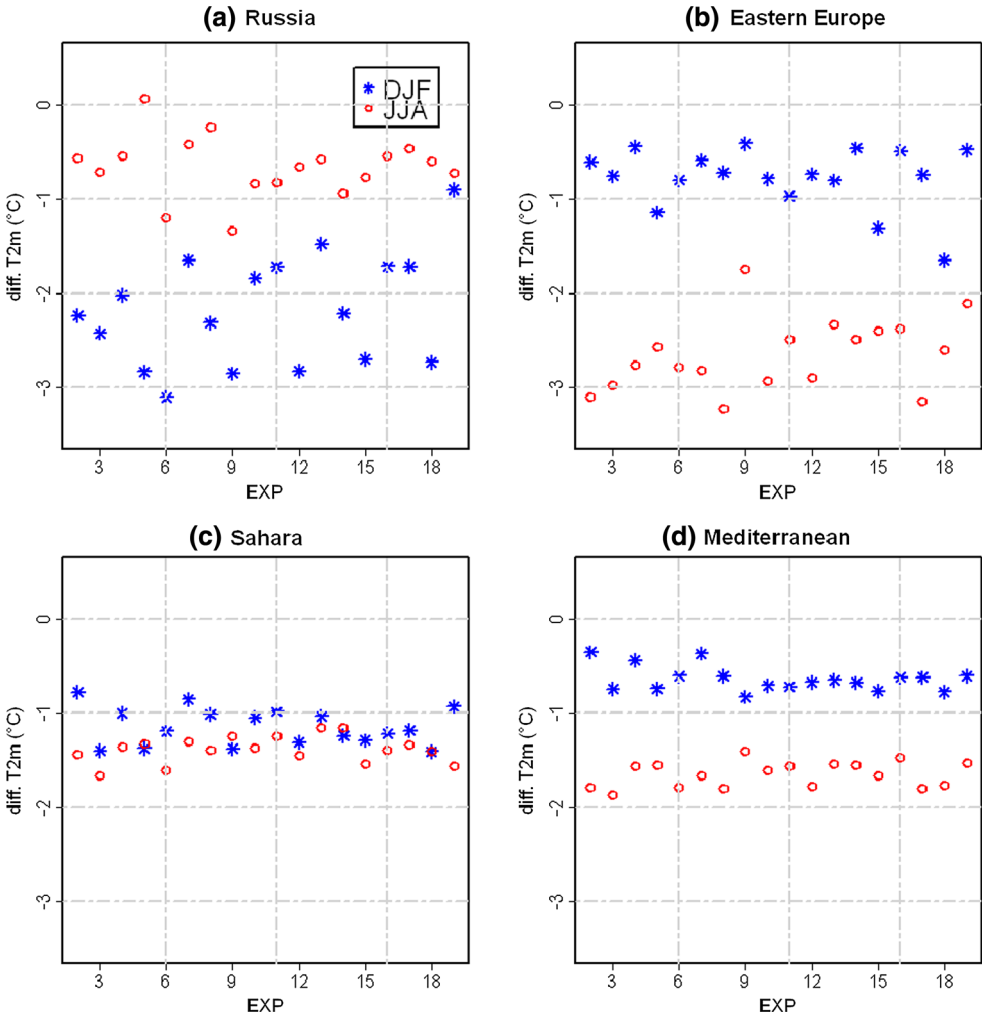

Fig. 9 Differences of 2 m air temperature *T2m* in an ensemble of UW PBL simulations relative to Holtslag simulation (EXP001) over four regions during DJF (*blue stars*) and JJA (*red circles*). The period analyzed is 1989–1991 and selected regions are shown in Fig. 1. Units are °C

Nevertheless, using the UW scheme, RegCM simulations are more in line with the ERA-Interim reanalysis in terms of water vapour mixing ratio, relative humidity and temperature vertical profiles (see Fig. S3 for the comparison of the vertical profiles of the selected variables on pressure levels over the Eastern Europe).

5 Perturbed physics ensemble of the UW simulations

In this section, the RegCM response in several near-surface variables is considered and compared with the default experiment (Holtslag scheme, EXP001) when three parameters (l, a_2 and R_{STBL}) in the UW scheme are varied according to the definitions from Table 1 (experiments EXP002 through EXP019). For all experiments, the comparison is based on the 3-year (1989–1991) averages.

In comparison with the default EXP001, the RegCM response in *T2m* to perturbations of the chosen parameters in the UW PBL scheme is almost unique: a temperature decrease in all experiments over all regions and in both DJF and JJA (Fig. 9). The amplitude of cooling reaches 3 °C over Eastern Europe during JJA and over Russia during DJF; this is consistent with the air temperature vertical profiles during JJA (Fig. 4d) and DJF (Fig. 4c). A negligible warming is detected only over Russia during JJA in EXP005. Larger differences during DJF than during JJA over Russia suggest that the UW scheme improves (since the bias is reduced) simulation of the stably stratified PBLs over this region. There is essentially no systematic grouping of different experiments according to perturbed parameters, except over Russia during winter (Fig. 9a) where the experiments with $R_{STBL} = 1.00$ (i.e. EXP003, 6, 9, 12, 15, 18) tend to be cooler than the other experiments, sometimes twice as much for the same efficiency a_2. Reduction of R_{STBL} and associated reduction of the master turbulent mixing length (cf. Eq. 8) in stably stratified conditions can induce less vertical mixing of the cool surface air and warmer air above, consistent with additional cooling found in experiments with $R_{STBL} = 1.00$. An inspection of vertical profiles reveals a dominant tropospheric cooling with the amplitude of up to 3 °C in all

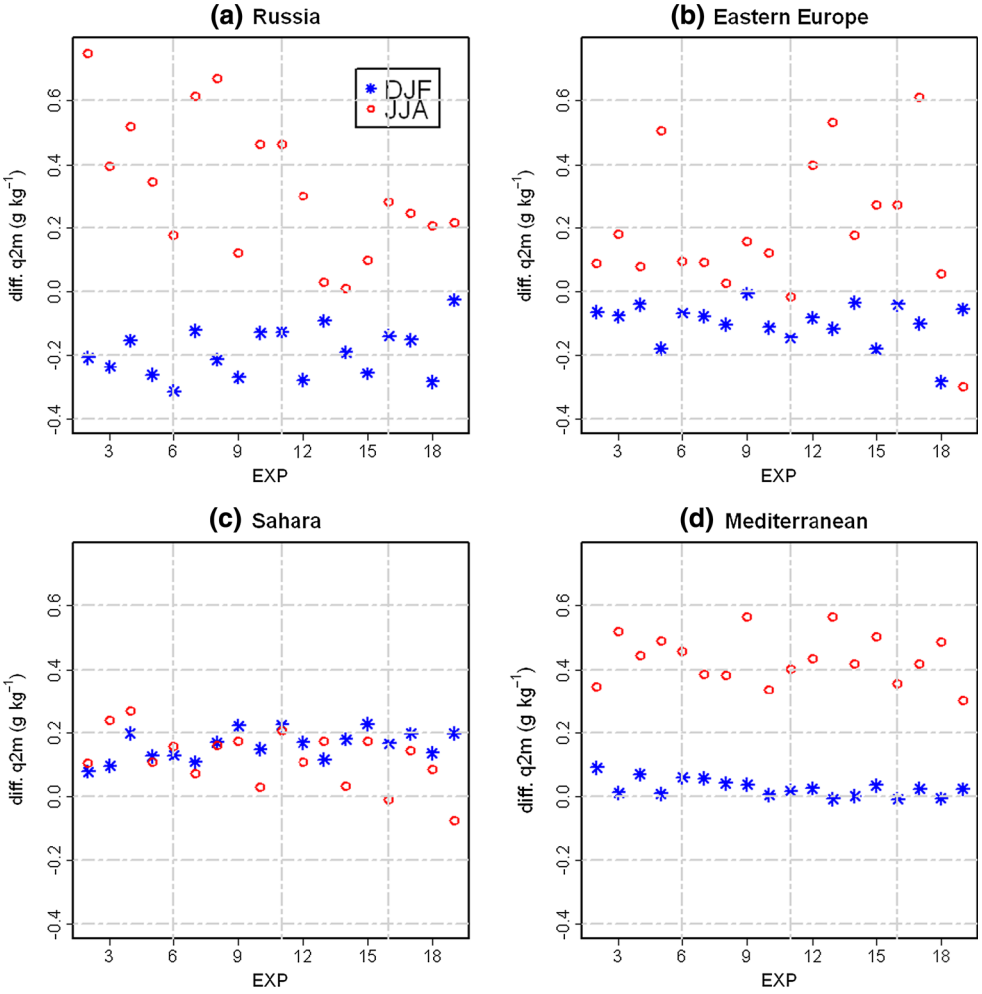

Fig. 10 Same as Fig. 9 but for the 2 m specific humidity *q2m*. Units are g kg^{-1}

members of the UW ensemble (not shown). This is comparable to the results of the 10-year UW experiment in Fig. 4.

The model response in terms of the 2 m specific humidity (*q2m*) is more complex than for *T2m* (Fig. 10). In JJA, a large majority of differences in the UW experiments are of the same sign, i.e. an increase of *q2m* in all regions is seen, consistent with the increased precipitation with the UW scheme (Fig. 3d). This is also consistent with an increase in water vapour mixing ratio *qv* over all regions during JJA and over dry regions Sahara and Mediterranean during DJF (Fig. 5c, d). During DJF, one can notice a consistent reduction of *q2m* in the UW experiments with the magnitude of up to 0.3 g kg^{-1} over Russia and Eastern Europe (cf. Fig. 5c).

From Fig. 10, three types of the *q2m* response can be identified and associated with the dominant *T2m* cooling of the UW scheme in Fig. 9. First, over Russia and Eastern Europe the opposite sign of the *q2m* changes is seen in DJF and in JJA respectively, accompanied with large spread, particularly in the summer. Second, over Sahara, *q2m* is increased in both seasons with moderate intra-ensemble spread. And third, over Mediterranean Fig. 10d shows a small increase in *q2m* during DJF and a substantial increase during JJA. The presence of a low intra-ensemble spread over Mediterranean is partially the consequence of the area smoothing since this is the largest region considered. The spread is larger during JJA when compared to DJF, but without clear grouping according to perturbed parameters. The only clear exception is found over Russia during winter (Fig. 10a) where the experiments with $R_{STBL} = 1.00$ tend to be drier than the other experiments. This can be associated again with a decrease in vertical mixing; this is expected when R_{STBL} is reduced (cf. Eq. 8).

When considering eddy heat diffusivity K_H, a strong sensitivity to the formulation of the master turbulent length scale l is found (Fig. 11). Here, eddy heat diffusivity at the first model level above ground is shown, but the same response is detected also at several higher levels (not shown, but it is consistent with K_H vertical profiles and differences between EXP001 and EXP002 in Fig. 6). The differences in K_H are largely grouped according to the choice of l; even over Russia in the winter there is a hint of such a grouping. The difference of -14 m^2 s^{-1} relative to

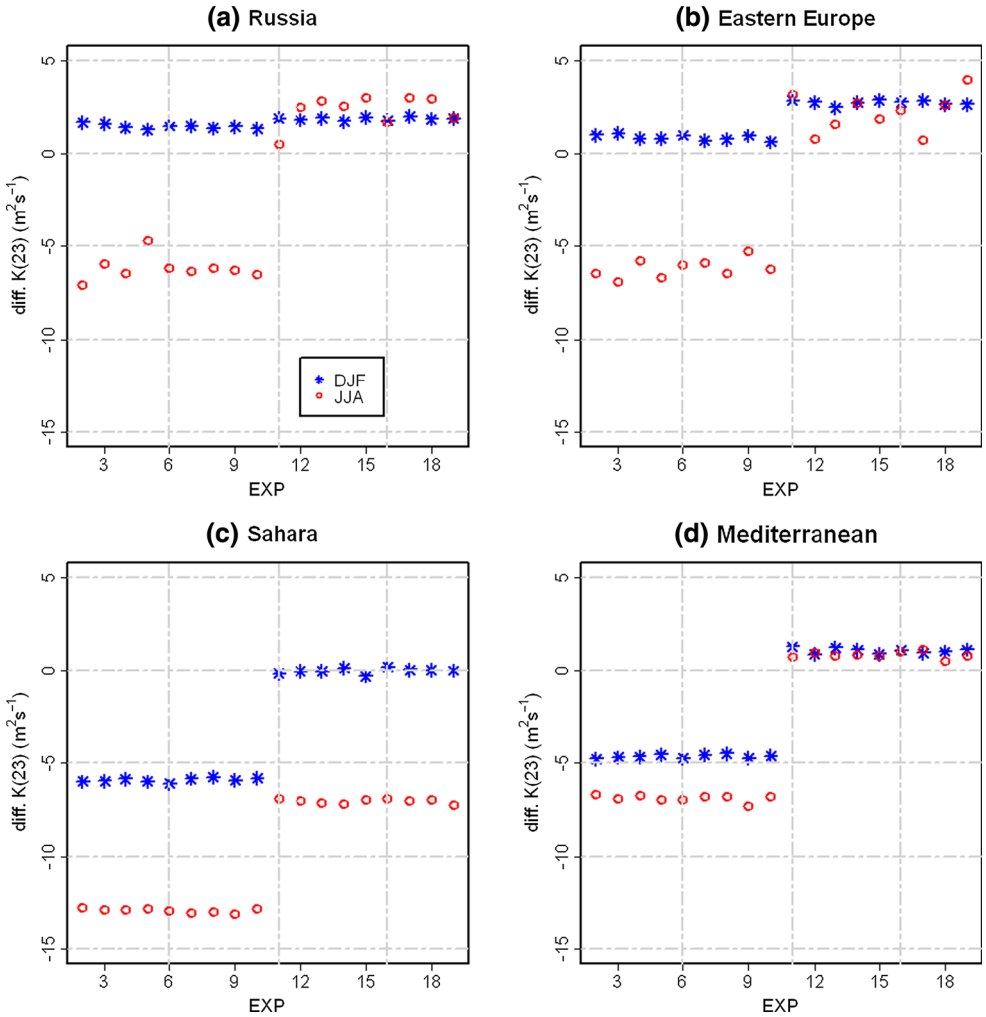

Fig. 11 Same as Fig. 9 but for eddy heat diffusivity K_H at the lowest model level. Units are $m^2\ s^{-1}$

the Holtslag scheme (EXP001) is reached when the l_1 formulation (Eq. 6) is used, as seen over Sahara during JJA; on the other hand, it can reach up to 4 $m^2\ s^{-1}$ when the l_2 formulation (Eq. 7) is used, as seen over Eastern Europe during JJA. In general, the use of l_1 yields the larger eddy heat diffusivity differences near the surface when compared to l_2. This may be expected from Eqs. (6) and (7). Again, as before, no clear grouping of simulations according to the two parameters (a_2 and R_{STBL}) is detected.

To summarize, the amplitude of the *T2m* and *q2m* differences in the experiments EXP003 to EXP019 does not differ dramatically from that in EXP002 (which is the default experiment for the UW scheme) and the spread among the UW experiments may be considered as relatively small to moderate. The spread in the UW ensemble and similarity of the responses over different geographic regions implies that the default parameter settings will likely yield similar results in simulations over other regions and time intervals. Although for certain combinations of parameters these differences may be occasionally larger than in EXP002, generally this is neither a systematic nor significant event. This may support the choice of the default a_2 and R_{STBL} (at least over the European domain). However, sensitivity of some aspects of model climatology (i.e. the K_H profiles) can motivate further research and implementation of e.g. more refined master turbulent mixing length scale formulations (e.g. Grisogono 2010).

6 Summary and conclusions

Sensitivity of the regional climate model RegCM4.2 to the choice of the PBL parameterisation was analyzed in this study. The two implemented PBL schemes were the Holtslag scheme (Holtslag et al. 1990) and the UW scheme (Grenier and Bretherton 2001). Furthermore, sensitivity of the UW scheme to different formulations of the master turbulent mixing length scale in unstably stratified conditions and to perturbations of two unconstrained parameters, associated with (a) the entrainment efficiency and (b) the formulation of the master turbulent length scale in stably stratified conditions, was also explored. The second type of

sensitivity test is performed by the method of perturbed physics ensemble (PPE).

Our results show that substantial changes in model climatology are possible when two different PBL parameterisations are used. When compared with the Holtslag scheme, the use of the UW scheme reduces *T2m* over the European and northern Africa land regions up to 3 °C, but mostly between 1 and 2 °C. This temperature reduction is, as expected, mostly confined to the model PBL but it also extends to the lower troposphere. The magnitude of the reduction of *T2m* was higher during JJA than in DJF, i.e. in the season with the strongest turbulent activity within PBL. When compared with the verifying CRU *T2m* data (and with precipitation during JJA), it was demonstrated that the use of the UW scheme in RegCM4.2 is beneficial: a substantial warm bias in the north-eastern Europe during DJF and the warm bias in central Europe during JJA are reduced. These improvements increase the model's fidelity in simulating very stable conditions in the subarctic parts of Europe during DJF. The UW scheme also contributes to a vertical redistribution of water vapour closer to ERA-Interim reanalysis. The effect of such redistribution is a spatially more coherent structure of the water vapour field during JJA, including an increase of the water vapour amounts in the lower troposphere and a decrease in the mid-atmospheric layers.

The differences between the two PBL schemes in terms of temperature and water vapour mixing ratio can be partially ascribed to the schemes' different vertical profiles of eddy heat diffusivity and associated tendencies induced by turbulent mixing. Eddy heat diffusivity is substantially reduced in the UW simulations relative to the control simulation with the Holtslag PBL scheme, especially during JJA. This reduction is not homogeneous in the vertical; the vertical slope of eddy heat diffusivity is also changed, resulting in the reduced temperature tendencies. Other possible sources of differences in (the temperature and water vapour) tendencies between two PBL schemes are found to be related to changes in the characteristics (slope and curvature) of vertical profiles of prognostic variables. Vertical profiles of the water vapour mixing ratio (*qv*) tendencies reveal a major increase of the PBL-generated *qv* tendency in the prognostic equation when the UW scheme was used. Since a PBL scheme impacts other model prognostic variables, a careful experimental design to study these impacts should include an analysis of model tendencies due to all simulated processes.

In terms of interaction between land surface and near-surface atmospheric fields, the evaluation of latent heat flux suggests that RegCM simulations with the UW scheme are not superior to those when the Holtslag scheme is employed, but the evaluation of sensible heat flux clearly indicates benefits of using the UW scheme (Supplement 2); however, this improvement is by no means unambiguous.

The PPE reveals that sensitivity to the formulation of the turbulent master mixing length scale in the UW scheme can be detected through the changing values of eddy heat diffusivity. However, our results indicate that the simulated near-surface temperature and specific humidity are relatively insensitive to the changes in its formulation. Furthermore, it was also demonstrated that the UW scheme is not very sensitive to the perturbations of two unconstrained parameters (the efficiency of evaporative enhancement of the cloud-top entrainment, a_2, and the scaling parameter in statically stable boundary layer turbulence length scale, R_{STBL}). However, an exception is found in the northern parts of the domain, where a reduction of the default value of R_{STBL} is systematically followed by the reduction of *T2m*. This supports the hypotheses that a reduction of the vertical mixing and temperature tendencies from the PBL scheme will result from the reduction of R_{STBL}. Since in both PBL schemes only the simplest formulations of the master mixing length scale are implemented, this question deserves further investigation. Also, in addition to the PPE methodology, a larger-scale systematic sensitivity might be detected by employing a statistical ensemble methodology (e.g. O'Brien et al. 2011).

Even among the diverse geographic regions considered in this study, our experiments show some common changes in the vertical profiles of eddy heat diffusivity, temperature, and water vapour tendency. This common response likely originates in the reduction of eddy heat diffusivity, which itself is partially due to the prognostic nature of the UW PBL scheme (e.g. Cuxart et al. 2006; Bretherton and Park 2009). The main results of this study include the following: (1) the UW parameterisation generally reduces lower tropospheric diffusivity; (2) the UW parameterisation generally decreases lower tropospheric temperatures (possibly due to reduced entrainment of potentially warm free tropospheric air into the boundary layer); and (3) the UW model produces water vapour tendencies that are systematically and dramatically higher than tendencies from the Holtslag model. While changes (1) and (2) are likely related, it is not immediately clear what causes change (3). It is clear however, that dynamical processes or other parameterisations must compensate for the increased water vapour tendency, since the simulations with the UW PBL do not exhibit a systematic increase in water vapour mixing ratio. Further study will be necessary to understand how model dynamics and parameterisations compensate for the systematic increase in water vapour mixing ratio (e.g. possibly an intercomparison using WRF with the UW PBL).

Although the current implementations of both PBL schemes in the RegCM model somewhat diverge from their original formulations, they are well situated for the regional climate studies. Our analyses explored only a part of

sensitivity induced by PBL parameterisation and showed that the use of the UW scheme is beneficial over regions of substantial warm and moderately dry biases. We expect an improvement in the near-surface temperature climatology in RegCM simulations using the UW scheme over other domains where winter warm biases are documented (e.g. Mearns et al. 2012; Ozturk et al. 2012). Any future analysis of the RegCM model uncertainties due to PBL schemes would benefit from intercomparison with other regional and global climate models with the aim to have physically realistic simulations of the near-surface climatology, systematic errors in a physically acceptable range and a climate model that can realistically reproduce observed feedbacks.

Acknowledgments ECMWF ERA-Interim data used in this study have been obtained from the ECMWF data server. University of East Anglia CRU data used in this study have been obtained from http://badc.nerc.ac.uk. Surface flux measurements from the EUMETNET organized C-SRNWP Project have been obtained from the COSMO consortium database (http://www.como-model.org/srnwp/content) and provided by the FMI, KNMI, DWD and Meteo-France. Computations and visualizations in this study have been performed using cdo (https://code.zmaw.de/projects/cdo), GrADS (http://www.iges.org/grads) and R (http://www.R-project.org/) software. Branko Grisogono is supported by the Croatian Ministry of Science, Education and Sports (MZOS) and Croatian Science Foundation through projects BORA-MZOS 119-1193086-1311 and CATURBO-HRZZ 09/151. Ivan Güttler and Čedo Branković are supported by the MZOS project 004-1193086-3035. The contribution by T.A. O'Brien was supported by the Director, Office of Science, Office of Biological and Environmental Research of the U.S. Department of Energy under Contract No. DE-AC02-05CH11231 as part of the Regional and Global Climate Modeling Program (RGCM). We thank to two anonymous reviewers for their constructive criticism, comments and suggestions that greatly improved the original manuscript.

References

Baklanov A, Grisogono B, Bornstein R, Mahrt L, Zilitinkevich S, Taylor P, Larsen S, Rotach M, Fernando HJS (2011) On the nature, theory, and modeling of atmospheric planetary boundary layers. Bull Am Meteor Soc 92:123–128

Bellprat O, Kotlarski S, Lüthi D, Schär C (2012) Exploring perturbed physics ensembles in a regional climate model. J Clim 25:4582–4599

Blackadar AK (1962) The vertical distribution of wind and turbulent exchange in a neutral atmosphere. J Geophys Res 67:3095–3102

Bretherton CS, Park S (2009) A new moist turbulence parameterization in the community atmosphere model. J Clim 22:3422–3448

Coppola E, Giorgi F, Mariotti L, Bi X (2012) RegT-Band: a tropical band version of RegCM4. Clim Res 52:115–133

Curry JA, Webster PJ (2011) Climate science and the uncertainty monster. Bull Am Meteor Soc 92:1667–1682

Cuxart J et al (2006) Single-column model intercomparison for a stably stratified atmospheric boundary layer. Bound-Layer Meteor 118:273–303

Davis N, Bowden J, Semazzi F, Xie L, Önol B (2009) Customization of RegCM3 regional climate model for eastern Africa and a tropical Indian Ocean domain. J Clim 22:3595–3616

Dee DP et al (2011) The ERA-Interim reanalysis: configuration and performance of the data assimilation system. Q J R Meteorol Soc 137:553–597

Dethloff K, Abegg C, Rinke A, Hebestadt I, Romanov VF (2001) Sensitivity of Arctic climate simulations to different boundary-layer parameterizations in a regional climate model. Tellus 53A:1–26

Dickinson RE, Henderson-Sellers A, Kennedy PJ (1993) Biosphere-atmosphere transfer scheme (BATS) version 1e as coupled to the NCAR community climate model. NCAR Tech. Note NCAR/TN-387 + STR, NCAR, Boulder, Colorado, USA, 72 pp

Emanuel KA (1991) A scheme for representing cumulus convection in large-scale models. J Atmos Sci 48:2313–2335

Esau I, Zilitinkevich S (2010) On the role of the planetary boundary layer depth in the climate system. Adv Sci Res 4:63–69

Galperin B, Kantha LH, Hassid S, Rosati A (1988) A quasi-equilibrium turbulent energy model for geophysical flows. J Atmos Sci 45:55–62

García-Díez M, Fernández J, Fita L, Yagüe C (2013) Seasonal dependence of WRF bias and sensitivity to PBL schemes over Europe. Q J R Meteorol Soc 139:501–514

Gianotti RL, Zhang D, Eltahir EAB (2012) Assessment of the regional climate model version 3 over the maritime continent using different cumulus parameterization and land surface schemes. J Clim 25:638–656

Giorgi F, Marinucci MR, Bates GT (1993) Development of a second-generation regional climate model (RegCM2). Part I: boundary-layer and radiative transfer processes. Mon Weather Rev 121:2794–2813

Giorgi F et al (2012) RegCM4: model description and preliminary tests over multiple CORDEX domains. Clim Res 52:7–29

Grenier H, Bretherton CS (2001) A moist PBL parameterization for large-scale models and its application to subtropical cloud-topped marine boundary layers. Mon Weather Rev 129:357–377

Grisogono B (2010) Generalizing 'z-less' mixing length for stable boundary layers. Q J R Meteorol Soc 136:213–221

Güttler I (2011) Reducing warm bias over the north-eastern Europe in a regional climate model. Croatian Meteorol J 44(45):19–29

Güttler I, Branković Č, Srnec L, Patarčić M (2013) The impact of boundary forcing on RegCM4.2 surface energy budget. Clim Change. doi:10.1007/s10584-013-0995-x

Holtslag AAM, Boville B (1993) Local versus nonlocal boundary-layer diffusion in a global climate model. J Clim 6:1825–1842

Holtslag AAM, Moeng C-H (1991) Eddy diffusivity and countergradient transport in the convective atmospheric boundary layer. J Atmos Sci 48:1690–1698

Holtslag AAM, de Bruijn EIF, Pan HL (1990) A high resolution air mass transformation model for short-range weather forecasting. Mon Weather Rev 118:1561–1575

Hu X-M, Nielsen-Gammon JW, Zhang F (2010) Evaluation of three planetary boundary-layer schemes in the WRF model. J Appl Meteor Climatol 49:1831–1844

Jaeger EB, Stöckli R, Seneviratne SI (2009) Analysis of planetary boundary layer fluxes and land-atmosphere coupling in the regional climate model CLM. J Geophys Res 114:D17106. doi:10.1029/2008JD011658

Kiehl J, Hack J, Bonan G, Boville B, Breigleb B, Williamson D, Rasch P (1996) Description of the NCAR community climate model (CCM3). NCAR Tech. Note NCAR/TN-420 + STR. NCAR, Boulder, Colorado, USA, 152 pp

Kim J, Waliser DE, Mattmann CA, Goodale CE, Hart AF, Zimdars PA, Crichton DJ, Jones C, Nikulin G, Hewitson B, Jack C, Lennard C, Favre A (2013) Evaluation of the CORDEX-Africa multi-RCM hindcast: systematic model errors. Clim Dyn. doi:10.1007/s00382-013-1751-7

Knight CG, Knight SHE, Massey N, Aina T, Christensen C, Frame DJ, Kettleborough JA, Martin A, Pascoe S, Sanderson B, Stainforth

DA, Allen MR (2007) Association of parameter, software, and hardware variation with large-scale behaviour across 57,000 climate models. Proc Natl Acad Sci USA 104:12259–12264

Kothe S, Ahrens B (2010) On the radiation budget in regional climate simulations for West Africa. J Geophys Res 115:D23120. doi:10.1029/2010JD014331

Mahrt L, Vickers D (2003) Formulation of turbulent fluxes in the stable boundary layer. J Atmos Sci 60:2538–2548

Mauritsen T, Svensson G, Zilitinkevich SS, Esau I, Enger L, Grisogono B (2007) A total turbulent energy closure model for neutrally and stably stratified atmospheric boundary layers. J Atmos Sci 64:4113–4126

Mearns LO, Arritt R, Biner S, Bukovsky MS, McGinnis S, Sain S, Caya D, Correia J Jr, Flory D, Gutowski W, Takle ES, Jones R, Leung R, Muofouma-Okia W, McDaniel L, Nunes AMB, Qian Y, Roads J, Sloan L, Snyder M (2012) The North American Regional Climate Change Assessment Program: overview of phase I results. Bull Am Meteor Soc 93:1337–1362

Medeiros B, Hall A, Stevens B (2005) What controls the mean depth of the PBL? J Clim 18:3157–3172

Mellor G, Yamada T (1982) Development of a turbulence closure model for geophysical fluid problems. Rev Astrophys Space Phys 20:851–875

Mitchell TD, Jones PD (2005) An improved method of constructing a database of monthly climate observations and associated high-resolution grids. Int J Climatol 25:693–712

Murphy JM, Sexton DMH, Barnett DN, Jones GS, Webb MJ, Collins M, Stainforth DA (2004) Quantification of modelling uncertainties in a large ensemble of climate change simulations. Nature 430:768–772

Nicholls S, Turton JD (1986) Observational study of the structure of stratiform cloud layers. Part II: entrainment. Q J R Meteorol Soc 112:461–480

Nieuwstadt FTM (1984) The turbulent structure of the stable, nocturnal boundary layer. J Atmos Sci 41:2202–2216

O'Brien TA, Sloan LC, Snyder MA (2011) Can ensembles of regional climate model simulations improve results from sensitivity studies? Clim Dyn 37:1111–1118

O'Brien TA, Chuang PY, Sloan LC, Faloona IC, Rossiter DL (2012) Coupling a new turbulence parametrization to RegCM adds realistic stratocumulus clouds. Geosci Model Dev Discuss 5:989–1008

Ozturk T, Altinsoy H, Türkeş M, Kuranz ML (2012) Simulation of temperature and precipitation climatology for the Central Asia CORDEX domain using RegCM 4.0. Clim Res 52:63–76

Pal JS, Small EE, Eltahir EA (2000) Simulation of regional-scale water and energy budgets: representation of subgrid cloud and precipitation processes within RegCM. J Geophys Res 105:D24, 29579–29594

Pielke RA Sr (2002) Mesoscale meteorological modeling, 2nd edn. Academic Press, San Diego, p 676

Sánchez E, Yagüe C, Gaertner MA (2007) Planetary boundary layer energetics simulated from a regional climate model over Europe for present climate and climate change conditions. Geophys Res Lett 34:L01709. doi:10.1029/2006GL028340

Shin S-H, Ha K-J (2007) Effects of spatial and temporal variations in PBL depth on a GCM. J Clim 20:4717–4732

Solmon F, Elguindi N, Mallet M (2012) Radiative and climatic effects of dust over West Africa, as simulated by a regional climate model. Clim Res 52:97–113

Stainforth DA et al (2005) Uncertainty in predictions of the climate response to rising levels of greenhouse gases. Nature 433:403–406

Stainforth DA, Allen MR, Tredger ER, Smith LA (2007) Confidence, uncertainty and decision-support relevance in climate predictions. Philos Trans R Soc Lond A365:2145–2161

Steiner AL, Pal JS, Giorgi F, Dickinson RE, Chameides WL (2005) The coupling of the common land model (CLM0) to a regional climate model (RegCM). Theor Appl Climatol 82:225–243

Steiner AL, Pal JS, Rauscher SA, Bell JL, Diffenbaugh NS, Boone A, Sloan LC, Giorgi F (2009) Land surface coupling in regional climate simulations of the West African monsoon. Clim Dyn 33:869–892

Stensrud D (2007) Parameterization schemes: keys to understanding numerical weather prediction models. Cambridge University Press, Cambridge, p 459

Stewart RW (1979) The atmospheric boundary layer, WMO no 523. World Meteorological Organization, Geneva, p 44

Stull RB (1988) An introduction to boundary layer meteorology. Kluwer, Dordrecht, p 666

Suklitsch M, Gobiet A, Truhetz H, Awan NK, Göttel H, Jacob D (2011) Error characteristics of high resolution regional climate models over the Alpine region. Clim Dyn 37:377–390

Sylla MB, Coppola E, Mariotti L, Giorgi F, Ruti PM, Dell'Aquila A, Bi X (2010) Multiyear simulation of the African climate using a regional climate model (RegCM3) with the high-resolution ERA-Interim reanalysis. Clim Dyn 35:231–247

Tebaldi C, Knutti R (2007) The use of the multi-model ensemble in probabilistic climate projections. Philos Trans R Soc Lond A365:2053–2075

Trenberth KE, Fasullo JT, Kiehl J (2009) Earth's global energy budget. Bull Am Meteor Soc 90:311–323

Troen IB, Mahrt L (1986) A simple model of the atmospheric boundary layer: sensitivity to surface evaporation. Bound-Layer Meteor 37:129–148

Van de Berg WJ, van den Broeke MR, van Meijgaard F (2007) Heat budget of the East Antarctic lower atmosphere derived from a regional atmospheric climate model. J Geophys Res 112:D23101. doi:10.1029/2007JD008613

Vautard R et al (2013) The simulation of European heat waves from an ensemble of regional climate models within the EURO-CORDEX project. Clim Dyn 41:2555–2575

Walter KM, Zimov SA, Chanton JP, Verbyla D, Chapin FS III (2006) Methane bubbling from Siberian thaw lakes as a positive feedback to climate warming. Nature 443:71–75

Winter JM, Pal JS, Eltahir EAB (2009) Coupling of integrated biosphere simulator to regional climate model version 3. J Clim 22:2743–2757

Winton M (2006) Surface albedo feedback estimates for the AR4 climate models. J Clim 19:359–365

Wyngaard JC (1985) Structure of the planetary boundary layer and implications for its modeling. J Clim Appl Meteorol 24:1131–1142

Xie B, Fung JCH, Chan A, Lau A (2012) Evaluation of nonlocal and local planetary boundary layer schemes in the WRF model. J Geophys Res 117:D12103. doi:10.1029/2011JD017080

Yang Z, Arritt RW (2002) Test of a perturbed physics ensemble approach for regional climate modeling. J Clim 15:2881–2986

Zhang Y, Xie S, Covey C, Lucas DD, Gleckler P, Klein SA, Tannahill J, Doutriaux C, Klein R (2012) Regional assessment of the parameter-dependent performance of CAM4 in simulating tropical clouds. Geophys Res Lett 39:L14708. doi:10.1029/2012GL052184

Zhu P et al (2005) Intercomparison and interpretation of single-column model simulations of a nocturnal stratocumulus-topped marine boundary layer. Mon Weather Rev 133:2741–2758